arXiv:2608.19491v2 [cs.LG] 3 Sep 2026

Activation-Keyed Momentum: An Anisotropic Momentum Update via the Delta Rule

Euijin Hong **Guannan Qu**
Electrical and Computer Engineering, Carnegie Mellon University
{ehong, gqu}@andrew.cmu.edu

Abstract

Most modern optimizers form their momentum as an exponential moving average (EMA) of past gradients, forgetting every direction at one fixed rate. However, the inputs a deep network sees during training can be highly anisotropic, with a few directions queried frequently while most are seen rarely. Preconditioning methods address this anisotropy by wrapping extra processing around this buffer and leave the momentum update itself unchanged. We propose Activation-Keyed Momentum (AK-MOMENTUM), which builds direction-awareness into the momentum update rule. The gradient of a linear layer splits into an input activation that acts as a *key* and an output-side error that acts as a *value*. Keying on that activation, AK-MOMENTUM updates the momentum buffer by the canonical delta rule, so each direction is forgotten at a rate set by how often it appears. We prove that it is a valid momentum, that it applies the input-side curvature correction without matrix inversion, and that it clears stale directions faster than EMA under both a fixed and a drifting optimum. It is a drop-in replacement for the momentum buffer of any optimizer, its coefficient transfers across widths under μP, and its extra compute stays between 22.2% and 25.0% of a gated-MLP block's linear cost with no persistent memory. In FineWeb-Edu pretraining, AdamW with AK-MOMENTUM (AK-AdamW) reaches AdamW's validation loss in up to $46.39 \pm 4.32\%$ fewer steps at 67M and $22.12 \pm 0.80\%$ at 370M over three seeds, and the gain persists at 1B on a Chinchilla-optimal budget. A Muon baseline tuned under the same protocol sits above AK-AdamW at both language-model scales, and the gain holds for SGD, ResNet-18, and ViT-Tiny on CIFAR-10. Training-time diagnostics confirm the predicted mechanism, better gradient tracking and healthier input directions.

1 Introduction

Training large neural networks is expensive, and much of the recent advancements in large-scale AI has come from optimizers that reach better solutions in fewer steps, enabling to train larger models on more data by more efficiently utilizing a fixed compute budget. The frontier has moved steadily, from Adam and AdamW [10, 12] to more recent methods such as Shampoo, SOAP, and Muon [8, 25, 9]. Underneath all of these optimizers, however, sits one component that has barely changed, the momentum. Every one of these optimizers keeps a running average of past gradients, its momentum, integrating each new gradient and forgetting older ones at a single fixed rate [18]. This exponential moving average (EMA) update rule of momentum is the part of the optimizer this paper rethinks.

In a neural network linear layer $y = Wx$, the gradient of a single data point separates cleanly into two pieces $g = \delta x^\top$: 1) the input x the layer just received and 2) the backpropagated error from loss $\mathcal{L}$, $\delta = \frac{\partial \mathcal{L}}{\partial y}$, to correct at its output. The first piece indicates where in the input space the layer received the signal, and the second says what corresponding correction to apply on the output space.

Preprint.

Following Behrouz et al. [3, 2], the two pieces in this perspective are exactly a key and a value, an address and the contents to store at that address. An EMA update of a standard momentum discards this structure. By averaging each gradient as a flat matrix and fading all of them at a single rate, the running average collapses the key-value pairing the gradient provides for free, throwing away which directions are being queried and how often, before the optimizer ever uses it.

This structure matters because real training is largely anisotropic across eigendirections of gradients. The input statistics of a layer and the curvature of the loss are dominated by a small portion of directions, followed by a long tail of directions that are nearly flat and rarely excited [20, 7, 16, 14, 6]. A single fixed forgetting rate can be problematic in both cases. On one hand, along directions that appear often, the newest gradients carry the freshest information, yet a fixed forgetting rate keeps the stale gradients at full weight. On the other hand, along directions that appear rarely, more averaging would suppress noise, yet they fade on the same short schedule as everything else. An ideal momentum update should determine the forgetting rate on how often a direction is actually seen, and a unified rate cannot deliver that.

The field recognizes this asymmetry, and strong optimizers such as K-FAC, Shampoo, and SOAP exist to address it. However, what they share is that the momentum update rule itself is left unchanged (see Related Work and Appendix B for a detailed discussion). The goal of this paper is to *address the feature anisotropy at the momentum level.*

Contribution. We propose AK-MOMENTUM (6), which builds this direction-awareness into the momentum update itself. Instead of fading every direction at a single rate, it treats the incoming input activation as a key, erases the stored content along the direction that key points to, and writes the new content there before moving on. Directions queried often are refreshed often and forgotten quickly, while directions queried rarely are left almost untouched and kept over long horizons, so the forgetting along each direction now follows how often that direction is seen. The rule behind this is the classical delta rule [27], the canonical method for storing key-value associations and the same mechanism used in recent associative-memory sequence models [21, 30], applied here to the momentum buffer with the input activation as the key.

The design is not just intuitive, it is provably well-behaved, and we establish three guarantees. First, AK-MOMENTUM remains a valid momentum, effectively tracking the gradient for gradient descent/ascent of an optimizer step (Theorem 3.4). Second, the correction AK-MOMENTUM applies resembles what curvature-based methods compute deliberately and at far higher cost (e.g. matrix inversion), enabled by its own correction term without inverting large matrices (Remark 3.6). Third, it clears stale directions strictly faster than a plain running average, both when the target is fixed (Theorem 3.8) and when the target itself drifts as the weights move (Theorem 3.10), which is what happens in practical neural network training.

Two further properties make AK-MOMENTUM practical rather than merely organized. AK-MOMENTUM is a drop-in replacement for the running-average momentum in any optimizer, leaving the second moment, weight decay, and any preconditioning exactly as they were. Thus it composes with methods like Shampoo, SOAP, and Muon rather than competing with them, since those act at a different level of the optimizer. Also, the idea is simple but the naive update form does not work as written, since it is unstable and breaks the clean transfer of settings across model sizes. Recovering both is achieved by normalizing the input key and working out the width-scaling, leaving a μP scaling law whose single new setting transfers across widths with no re-tuning and whose extra compute is small and well-characterized.

We test these theoretical advantages on language model pretraining at 67M, 370M, and 1B parameters on FineWeb-Edu [17]. The comparison is deliberately controlled against AdamW, the baseline that differs from our method only in the momentum update, so any difference in the loss curve is attributable to the change in momentum update. AK-MOMENTUM reaches AdamW's validation loss in up to $46.39 \pm 4.32\%$ fewer steps at 67M and $22.12 \pm 0.80\%$ fewer at 370M, and continues to a lower final loss, a gain that comfortably exceeds its compute overhead. The sign of the gap is the same in every run we report, and it holds at 1B on a Chinchilla-optimal token budget with every setting carried over from the 67M sweep. We also report a tuned Muon baseline, which sits above AK-AdamW at both language-model scales. The same pattern holds for a plain SGD variant on CIFAR-10 and for ResNet-18 and ViT-Tiny on the same dataset, confirming that the effect is not tied to Adam or to language modality, and a set of training-time diagnostics confirms that the

predicted mechanism, better gradient tracking property and healthier input directions, is what drives the improvement.

Related Work. Three lines of work are closely related to ours.

Preconditioning-based optimizers. K-FAC, Shampoo, and SOAP precondition the gradient using curvature information, and Muon post-processes the momentum to balance its directions [13, 8, 25, 9]. What they share is the level at which they act. Each keeps the running-average momentum and wraps extra processing around it, before the update or after, rather than changing the averaging rule. AK-MOMENTUM changes that momentum rule instead, and can be used in combination with these modern optimizers.

Input-side preconditioning. DoPr and Newton-Muon [31, 5] build a preconditioner from the second moment of the input activations and apply it to the momentum. That is the same input-side factor AK-MOMENTUM reaches implicitly, but AK-MOMENTUM does not need matrix inversion or any state beyond the momentum the base optimizer already keeps.

Optimizers as associative memory. Behrouz et al. [3, 2] view the optimizer and its momentum as an associative memory over past gradients, with the input activation as the key and the local error as the value. However, their motivation is memory capacity over long horizons rather than feature anisotropy. Their buffer-level rule keys on the gradient object rather than on its two factors, so a direction is forgotten at a rate set by the size of the error rather than how often that direction is seen. In comparison, AK-MOMENTUM keys on the input activation, which is what binds the forgetting rate to input density. Also related, Wang et al. [26] acts at the same level but compresses the buffer by low-rank approximation rather than through an associative-memory objective. Appendix B provides a detailed comparison of the rules side by side.

2 Background

Notations. In step t, the optimizer holds parameters θ_t and momentum M_{t-1} from the previous step, computes the gradient $g_t = \nabla_\theta L_t(\theta_t)$, updates momentum to M_t and parameters to θ_{t+1}.

2.1 EMA Momentum and Rank-1 Factorization of Gradients

EMA momentum's update rule is

$$M_t^{\mathrm{EMA}} = \beta M_{t-1}^{\mathrm{EMA}} + (1-\beta)\, g_t, \tag{1}$$

with momentum decay $\beta \in [0, 1)$. For a single linear layer $y = Wx$ with weight $W \in \mathbb{R}^{m\times n}$, input $x \in \mathbb{R}^n$ and output-side error $\delta = \partial L/\partial y \in \mathbb{R}^m$, the per-sample gradient *factorizes* as rank-1 outer product

$$g_t = \delta_t x_t^\top \in \mathbb{R}^{m\times n}. \tag{2}$$

This factored form is the structural fact that the rest of the paper exploits: it identifies x_t as a natural *key* and δ_t as a natural *value*, and turns the momentum buffer into an associative memory whose contents are precisely the historical (key, value) associations. We note that the key-value viewpoint of the factored gradient and the momentum buffer was proposed in recent work [3, 2], though their momentum buffer-level algorithm differs from ours in terms of which part is treated as key and which part is treated as value (see Appendix B for detailed discussion).

2.2 The Delta Rule

The classical delta rule (Widrow–Hoff, LMS) updates a matrix $M \in \mathbb{R}^{m\times n}$ to associate input keys $k \in \mathbb{R}^n$ with target values $v \in \mathbb{R}^m$ via

$$M \leftarrow M + \eta\,(v - Mk)\, k^\top, \tag{3}$$

where the residual $v - Mk$ is the *retrieval error*. In the fast-weight-programmer reformulation for sequence modeling, a memory matrix stores key–value pairs $\{(k_\ell, v_\ell)\}$. A purely Hebbian accumulator $M_t = M_{t-1} + v_t k_t^\top$ accumulates interference, while the delta-rule accumulator

$$M_t = M_{t-1} + \eta\,(v_t - M_{t-1}k_t)\, k_t^\top = M_{t-1}(I_n - \eta k_t k_t^\top) + \eta v_t k_t^\top \tag{4}$$

removes the old association at k_t before writing the new one, and provably preserves the orthogonality structure of stored memory [21, 30].

Under the delta rule, M is a linear associative memory that stores key–value pairs through least squares,

$$M_\star = \arg\min_M \frac{1}{2} \sum_{\ell=1}^{t} \|v_\ell - M k_\ell\|_2^2, \tag{5}$$

with the per-step update (3) performing one online SGD step on the per-sample term. We now apply this online associative-memory mechanism to the optimizer's momentum buffer to design AK-MOMENTUM in the next section.

3 AK-MOMENTUM: Methodology

The core proposed AK-MOMENTUM update rule is written as follows

AK-MOMENTUM UPDATE RULE.

$$M_t = \beta M_{t-1} + \eta \left(\delta_t - M_{t-1} x_t\right) x_t^\top, \tag{6}$$

with EMA decay $\beta \in [0, 1)$ and delta-rule correction coefficient $\eta \in (0, 1]$. Setting $\beta = 1$ recovers the pure delta rule. Factoring out M_{t-1} yields an equivalent form used throughout the analysis:

$$M_t = M_{t-1}\left(\beta I_n - \eta\, x_t x_t^\top\right) + \eta\, \delta_t x_t^\top. \tag{7}$$

The right-multiplying operator $\beta I - \eta x_t x_t^\top$ is a *data-dependent* forgetting factor that contracts directions aligned with the current key x_t and leaves orthogonal directions untouched, while the additive term $\eta \delta_t x_t^\top$ injects the new association. Equation (7) is the conceptual centerpiece, since every downstream property of AK-MOMENTUM is a property of the operator $\beta I - \eta x_t x_t^\top$.

The algorithm we deploy uses the normalized key $\hat{x}_t = x_t / \|x_t\|_2$ in place of x_t in (6), writing $\hat{\Sigma} := \mathbb{E}[\hat{x}\hat{x}^\top]$ for its second moment and $\hat{G} := \mathbb{E}[\delta \hat{x}^\top]$ for the matching gradient, which is what gives input-scale-independent stability and width transfer (Appendix C and Appendix Q).

Rationale: online key–value gradient memory. The starting observation is independent of any optimizer choice. As we mentioned in (2), the per-sample gradient of any linear layer $y = Wx$ factorizes as a rank-1 outer product $g_t = \delta_t x_t^\top$, where $x_t \in \mathbb{R}^n$ is the input activation and $\delta_t = \partial \mathcal{L} / \partial y_t \in \mathbb{R}^m$ is the output-side error. The two factors carry distinct roles. The key x_t identifies *where* in input space the layer received signal at step t, and the value δ_t specifies *what correction* to apply at that location. So (x_t, δ_t) is naturally a key–value pair, and the per-sample gradient itself is a rank-1 association.

The standard EMA accumulator $M_t = \beta M_{t-1} + (1-\beta) g_t$ averages these rank-1 outer products as if they were unstructured matrices, applying the same scalar decay β along every direction. We instead use the classical *delta rule* [27], the canonical online algorithm for storing key–value associations. Given a target value v at key k, it updates $M \leftarrow M + \eta\,(v - Mk)\, k^\top$, where $v - Mk$ is the *retrieval error*, the gap between the desired value at key k and the value the matrix currently retrieves. This update is exactly an online stochastic-gradient step on the function-space prediction loss $\frac{1}{2}\|v - Mk\|^2$.

The AK-MOMENTUM (6) is designed from the above delta-rule by identifying $v_t \leftrightarrow \delta_t$ and $k_t \leftrightarrow x_t$, and augmenting with a uniform decay β to retain an EMA-style longer memory horizon along untouched directions. The factored form (7) then reads as: *rather than averaging gradients as flat matrices,* AK-MOMENTUM *stores associations* (x_t, δ_t) *in* M *and updates them by the delta rule*, with the data-conditioned forgetting operator $\beta I - \eta\, x_t x_t^\top$ erasing stored content along the direction of the current key before writing the new association. Every subsequent property that we discuss in Sections 3.1–3.4, meaning the fixed point, the memory horizons, and the tracking dynamics, follows from this contractive operator.

Modular instantiations. AK-MOMENTUM is a replacement for the first-moment buffer of any base optimizer. SGD applied with AK-MOMENTUM (AK-SGD) applies (6) as the momentum buffer, followed by $\theta_{t+1} = \theta_t - \alpha M_t$. AdamW applied with AK-MOMENTUM (AK-AdamW) applies (6) to the first moment, while the second moment $v_t = \beta_2 v_{t-1} + (1-\beta_2) g_t^{\odot 2}$, bias correction, and decoupled weight decay are unchanged, with preconditioned update $U_t = \hat{M}_t \oslash (\sqrt{\hat{v}_t} + \varepsilon)$.

μP-clean width transfer. AK-MOMENTUM is μP-compatible. With the normalized key $\hat{x}_t$, the spectral norm of the rank-1 forgetting operator is $\|\hat{x}_t \hat{x}_t^\top\|_{\mathrm{op}} = 1$ independent of layer width, so the delta-rule coefficient η is width-invariant. Concretely, Theorem Q.1 (Appendix Q) shows that under maximal-update parameterization, the recurrence (6) admits a fixed-point per-coordinate scale of $\Theta(n^{-1/2})$ iff $\eta = \Theta(1)$, which is the same per-coordinate scale that EMA buffer attains and that the base optimizer's μP learning-rate rule expects. The base μP learning-rate rule is therefore inherited unchanged, with $\alpha = \Theta(1/n)$ for AK-AdamW (matching AdamW), $\Theta(1)$ for AK-SGD on hidden layers (matching SGD-momentum). The practical consequence is zero-shot hyperparameter transfer across widths, which we verify with a coordinate check at widths $\{128, 256, 512, 1024, 2048\}$ (Appendix S). The marginal tuning cost over EMA momentum is one coefficient, and we provide the recommended recipe and the evidence behind it (Appendix T).

FLOPs and memory. The per-step cost of (7) is one matrix–vector product $M_{t-1}x_t$ at $O(mn)$ and one outer-product update at $O(mn)$, matching EMA up to a constant factor. Against EMA (1), the extra work in the deployed normalized-key AK-MOMENTUM is the correction $\eta M \hat{\Sigma}$ together with the weight gradient that the standard AdamW second moment consumes. Per transformer block, taking the cheapest contraction order based on the shape of each layer, the correction costs $(6+4\gamma)/(24+18\gamma)$ of the linear forward and backward, where γ is the gated-MLP expansion ratio. The cost of the correction is strictly decreasing in γ, so it stays between 22.2% and 25.0% for any shape and sits at 23.1% for the Llama-2 ratio used in our experiments. Measured on actual runs, the realized per-step overhead is 11.2% at 67M and 17.4% at 370M. The measured costs are below the block-level band, since attention, embeddings, and the output head carry no delta-rule work and dilute the cost ratio, rising with width toward the calculated per-block cost band. Appendix L states the batch form of the deployed rule that produces every number we report, and Appendix M gives the full FLOPs and memory count, the per-layer dispatch rule, and the measurement setup. Persistent optimizer-state memory overhead is zero (no extra buffers beyond the momentum required by the base optimizer), and transient memory is bounded by $4Nn_{\max}$ per block.

We organize the remaining parts of this section around three questions. Section 3.1 establishes *why* AK-MOMENTUM *is valid* as a momentum buffer. Section 3.2 proves the bridging lemma that explains *why it is better than EMA*. Sections 3.3–3.4 derive the two principal consequences, faster per-direction convergence and direction-selective tracking under distribution shift, as corollaries of the same bridging lemma from Section 3.2. All symbols and notation used throughout are provided in Appendix A.

3.1 AK-MOMENTUM is a Valid Gradient Estimator

We establish why AK-MOMENTUM is a valid choice for the first-moment buffer despite departing from the standard EMA averaging objective. We first observe that any momentum buffer is, to first order in the learning rate, an estimator of the population gradient $\bar{G}(\theta_t) = \nabla_\theta \mathcal{L}(\theta_t)$, meaning the gradient of the expected loss over the data distribution rather than that of any single minibatch. Then, we identify the loss whose minimization defines AK-MOMENTUM and characterize its fixed point.

Remark 3.1 (Normalized-key substitution)**.** The results in this section are stated for the original AK-MOMENTUM (7). Every result from here on depends on the key only through its second moment. For the normalized-key version of AK-MOMENTUM, the whole analysis holds under substituting $\Sigma_x \to \hat{\Sigma}$, $\bar{G} \to \hat{G}$, and $\lambda_i \to \hat{\lambda}_i$. Since $\hat{\Sigma}$ has unit trace, $\hat{\lambda}_i$ lies in $[0, 1]$ and reads as the directional density of the input rather than its energy (Proposition C.1). Two places need more than the substitution and we flag them where they occur, which are the convergence point of (11) and the trace of (15).

Momentum buffer should effectively minimize the population gradient estimation loss. A first-order Taylor expansion of $\mathcal{L}$ at θ_t along the direction $-\alpha M_t$ gives, for any realization of M_t,

$$\mathcal{L}(\theta_t) - \mathcal{L}(\theta_t - \alpha M_t) = \alpha \langle M_t, \bar{G}(\theta_t) \rangle_F + O(\alpha^2), \tag{8}$$

where $\bar{G}(\theta_t) = \nabla_\theta \mathcal{L}(\theta_t)$ is the population gradient. This Taylor identity shows that any momentum buffer whose realized value deviates from $\bar{G}_t$ pays a first-order penalty $\alpha \langle \bar{G}_t - M_t, \bar{G}_t \rangle_F$, so the quality of M_t as an estimator of $\bar{G}_t$ directly governs optimization efficiency. The full statement and proof are deferred to Appendix D. What distinguishes EMA from AK-MOMENTUM is therefore not whether they are gradient estimators, but *which loss the buffer minimizes online* en route to that estimate.

Two natural objectives, two distinct fixed points. The pure delta rule (6) performs online stochastic gradient descent on the function-space prediction loss $\frac{1}{2}\|\delta - Mx\|^2$, while EMA (1) performs online stochastic gradient descent on the weight-space matrix loss $\frac{1}{2}\|M - g\|_F^2$. Both losses encode different questions about M, which we make precise below. The factored gradient $g_t = \delta_t x_t^\top$ admits two natural mean-square estimation objectives.

Definition 3.2 (Weight-space MSE)**.** $J_w(M) := \frac{1}{2}\mathbb{E}\big[\|M - \delta x^\top\|_F^2\big]$.

Definition 3.3 (Function-space prediction)**.** $J_f(M) := \frac{1}{2}\mathbb{E}\big[\|\delta - Mx\|_2^2\big]$.

The two have different closed-form minimizers: $M_w^\star = \bar{G}$ and $M_f^\star = \bar{G}\Sigma_x^{-1}$ when $\Sigma_x \succ 0$ (proof in Appendix E.1), and they coincide iff $\Sigma_x = cI$. Under stationarity, EMA's online SGD on J_w converges in expectation to $\bar{G}$, which is an unbiased estimator of the population gradient, while the pure delta rule's online SGD on J_f converges to $\bar{G}\Sigma_x^{-1}$, which is the Wiener-optimal linear predictor of δ given x (proof in Appendix E.2).

The Tikhonov-regularized Wiener fixed point of AK-MOMENTUM. Combining the delta-rule correction with a uniform decay $\beta < 1$ produces a regularized version of the Wiener predictor.

Theorem 3.4 (Fixed point of AK-MOMENTUM)**.** *Under the quasi-static approximation (parameters change slowly relative to the momentum dynamics, so $\bar{G}$ and Σ_x are treated as constant) and $\rho(\beta I - \eta\Sigma_x) < 1$, the* AK-MOMENTUM *update* (6) *converges in expectation to*

$$M^\star = \eta\, \bar{G}\left((1-\beta)I + \eta\Sigma_x\right)^{-1}. \tag{9}$$

In the eigenbasis of Σ_x,

$$M^\star u_i = \phi_i\, \bar{G} u_i, \qquad \phi_i = \frac{\eta}{(1-\beta) + \eta\lambda_i} = \frac{1}{\mu + \lambda_i}, \qquad \mu := \frac{1-\beta}{\eta}. \tag{10}$$

Proof. Take expectations of (7). At stationarity $M^\star\big((1-\beta)I + \eta\Sigma_x\big) = \eta\bar{G}$. See Appendix E.3. □

Corollary 3.5 (Fixed point of the deployed algorithm)**.** *For the normalized-key update the same computation gives*

$$M^* = \eta\, \hat{G}\left((1-\beta)I + \eta\hat{\Sigma}\right)^{-1} = \hat{G}\,(\mu I + \hat{\Sigma})^{-1}, \qquad M^* u_i = \frac{\hat{G}u_i}{\mu + \hat{\lambda}_i}. \tag{11}$$

When the key magnitude $\|x\|$ is independent of the pair $(\hat{x}, \delta)$, then $\hat{G} \propto \bar{G}$ and $\hat{\Sigma} \propto \Sigma_x$, so (11) is the unnormalized fixed point with a rescaled delta step, and the leftover scalar is absorbed by the learning rate. Without that condition, the buffer estimates a magnitude-reweighted gradient, in which directions carrying larger input norm are weighted more heavily. The condition holds exactly when $\|x\|$ is deterministic, which pre-normalization transformers enforce at every linear layer reading directly from an RMSNorm output [24]. Elsewhere it is an approximation, and the results that follow use the key only through its second moment, so none of them depends on it.

Table 1 compares the three estimator targets in the eigenbasis of Σ_x. The fixed point (10) interpolates monotonically between the two limits as μ varies. $\mu \to 0$ (i.e., $\beta \to 1$) yields $\phi_i \to 1/\lambda_i$, recovering the unregularized Wiener predictor. $\mu \to \infty$ (i.e., $\eta \to 0$) yields $\phi_i/\phi_j \to 1$, recovering EMA's direction-uniform scaling. AK-MOMENTUM thus sits naturally between EMA (direction-uniform) and Wiener (input-whitening), parameterized by the single ratio μ.

Table 1: Three estimator targets and their per-direction scaling of $\bar{G}u_i$ in the eigenbasis of Σ_x. The Tikhonov ridge is $\mu = (1-\beta)/\eta$.

Estimator	$M^\star u_i / \bar{G} u_i$	Description
EMA	1	Unbiased estimator of $\bar{G}$
Wiener ($\bar{G}\Sigma_x^{-1}$)	$1/\lambda_i$	Optimal linear predictor of δ given x
AK-MOMENTUM	$\phi_i = 1/(\mu + \lambda_i)$	Tikhonov-regularized Wiener

Remark 3.6 (K-FAC connection)**.** The Kronecker-factored Fisher approximation of a linear layer is $F \approx \mathbb{E}[\delta\delta^\top] \otimes \mathbb{E}[xx^\top]$, with natural-gradient update $\mathbb{E}[\delta\delta^\top]^{-1}\bar{G}\Sigma_x^{-1}$. The pure delta-rule fixed point $\bar{G}\Sigma_x^{-1}$ is exactly the input-side factor of this Kronecker product, so AK-MOMENTUM implements *implicit input-side natural-gradient preconditioning* without inverting Σ_x, at the cost of a single rank-one update per step rather than a layer-wise covariance inversion. The deployed algorithm whitens $\hat{\Sigma}$ rather than Σ_x, so this identification holds up to a scalar factor, given in Corollary 3.5.

Regarding (9) as an estimate of δ from x and interpreting the same expression as the gradient $\hat{G}$ right-multiplied by the preconditioner $(\hat{\Sigma} + \mu I)^{-1}$ are descriptions of the same object in two coordinate systems, and Appendix E.5 demonstrates this. Appendix K accounts for how the delta correction interacts with the second moment of Adam within AK-AdamW.

3.2 Anisotropic Memory Transport: The Unifying Lemma

We now prove a single bridging identity from which the steady-state, per-direction convergence, and non-stationary advantages of AK-MOMENTUM all follow as corollaries.

Iterating (7) with $M_0 = 0$ yields a closed-form expansion of M_t as a sum of past error–key outer products, each transported forward in time by a product of data-dependent contractions:

$$M_t = \eta \sum_{\ell=1}^{t} \delta_\ell x_\ell^\top \underbrace{\prod_{j=\ell+1}^{t} \left(\beta I_n - \eta x_j x_j^\top\right)}_{P_{\ell\to t} \in \mathbb{R}^{n\times n}}, \tag{12}$$

with $P_{t\to t} = I_n$. Each term $\eta\delta_\ell x_\ell^\top P_{\ell\to t}$ is the fading memory of the association stored at step ℓ. Along directions orthogonal to every subsequent key, $P_{\ell\to t}$ reduces to $\beta^{t-\ell} I$, a uniform geometric decay. Along directions aligned with subsequent keys, the additional factor $-\eta x_j x_j^\top$ applies a direction-selective attenuation, erasing stale content that conflicts with newly arriving keys.

Lemma 3.7 (Anisotropic memory transport)**.** Treat $\{x_j\}_{j>\ell}$ as drawn independently from a distribution with zero mean and covariance $\Sigma_x = \mathbb{E}[xx^\top] = \sum_i \lambda_i u_i u_i^\top$ where λ_i's are the eigenvalues and u_i's are the corresponding unit eigenvectors. Then

$$\mathbb{E}[P_{\ell\to t}]\, u_i = (\beta - \eta\lambda_i)^{t-\ell} u_i = \tilde{\beta}_i^{\,t-\ell} u_i, \qquad \tilde{\beta}_i := \beta - \eta\lambda_i. \tag{13}$$

Proof. By independence, $\mathbb{E}[P_{\ell\to t}] = \prod_{j=\ell+1}^{t} \mathbb{E}[\beta I - \eta x_j x_j^\top] = (\beta I - \eta\Sigma_x)^{t-\ell}$. Eigendecomposing Σ_x gives (13). □

Lemma 3.7 states that the expected memory of the buffer along direction u_i decays geometrically at rate $\tilde{\beta}_i$, with memory horizon

$$\tau_i = \frac{1}{1-\tilde{\beta}_i} = \frac{1}{(1-\beta) + \eta\lambda_i}. \tag{14}$$

High-density directions (with large λ_i) are forgotten more quickly, whereas low-density directions (with $\lambda_i \approx 0$) retain a longer EMA-like memory horizon $\approx 1/(1-\beta)$. *This direction-dependent memory horizon is the unifying mechanism behind every result that follows.*

Lemma 3.7 implies steady-state, per-direction convergence, and non-stationary advantages. The steady-state implication is Theorem 3.4, where the steady-state ratio of injection to forgetting along u_i is $\eta/[(1-\beta) + \eta\lambda_i] = \eta\tau_i$. The per-direction convergence and non-stationary implications follow as direct corollaries in Sections 3.3 and 3.4.

3.3 Faster Per-Direction Convergence

We compare how fast AK-MOMENTUM and EMA drive the parameter error to zero along each input direction. Linear regression is where the comparison can be made exactly, and there the per-direction iteration matrix of AK-MOMENTUM has strictly smaller determinant than that of EMA, yielding faster per-direction convergence in the underdamped regime. The determinant that drives the comparison never uses the squared loss, so the same statement carries to settings well beyond it, which we set out at the end of this subsection.

Setup Consider the population objective $\mathcal{L}(W) = \frac{1}{2}\mathbb{E}[\|Wx - y\|^2]$ with $y = W_\star x$ and $x \sim \mathcal{D}_x$ with covariance Σ_x. Letting $E_t = W_t - W_\star$, the dynamics decouple along the eigenbasis of Σ_x, where we let $e_{t,i} = E_t u_i \in \mathbb{R}^m$, $\mu_{t,i} = M_t u_i \in \mathbb{R}^m$, into per-direction 2×2 iteration matrices acting on $(e_{t,i}, \mu_{t-1,i})^\top$:

$$A_i^{\mathrm{EMA}} = \begin{pmatrix} 1 - \alpha(1-\beta)\kappa_i & -\alpha\beta \\ (1-\beta)\kappa_i & \beta \end{pmatrix}, \qquad A_i^{\mathrm{Delta}} = \begin{pmatrix} 1 - \alpha\eta\kappa_i & -\alpha\tilde{\beta}_i \\ \eta\kappa_i & \tilde{\beta}_i \end{pmatrix}, \tag{15}$$

where $\tilde{\beta}_i = \beta - \eta\hat{\lambda}_i$ and $\kappa_i = u_i^\top \mathbb{E}[\|x\|\, \hat{x}\hat{x}^\top] u_i$, under the hypothesis that $\hat{\Sigma}$ and $\mathbb{E}[\|x\|\, \hat{x}\hat{x}^\top]$ share eigenvectors so that the two split along the same directions (proof in Appendix F.1). Normalizing the key splits one parameter into two, since the buffer forgets at a rate set by the directional density $\hat{\lambda}_i$ while the parameter error still enters through the raw input, whose per-direction size is κ_i. The split is confined to the trace. The determinant depends only on $\hat{\lambda}_i$, which is why the two results below are unaffected by it. We write the EMA row with the same coupling so that the two rows are read side by side, and Theorem 3.8 shows the determinant does not depend on which coupling either row carries.

From this we derive the determinant reduction per-direction of A_i^{Delta} over A_i^{EMA}.

Theorem 3.8 (Per-direction determinant reduction)**.** *For all $\eta > 0$ and $\hat{\lambda}_i > 0$, $\det(A_i^{\mathrm{Delta}}) = \tilde{\beta}_i = \beta - \eta\hat{\lambda}_i < \beta = \det(A_i^{\mathrm{EMA}})$, and neither determinant depends on the coupling κ_i.*

Proof. Direct computation is shown in Appendix F.2. The result is a direct consequence of Lemma 3.7, since the expected per-direction memory contraction is exactly $\tilde{\beta}_i$. □

Extension beyond Linear Regression. The claim is not confined to the linear regression setting. The quantity that drives it never uses the squared loss, so the same comparison runs in high-dimensional linear regression with more input dimensions than samples and in canonical generalized linear models including logistic regression. Appendices I.2 and I.3 work out what the per-direction determinant reduction gives in these two settings, and Lemma 3.9 below is the mechanism that enables the extension.

The extension works because the loss enters Theorem 3.8 at exactly one place. In (15) the parameter error is coupled into the buffer through the single scalar $\eta\kappa_i$, where κ_i is the curvature of the squared loss along u_i. A different loss changes that scalar but not where it enters, so we focus on what the determinant does when the coupling is generalized to an arbitrary positive constant c instead of the value the squared loss prescribes.

Lemma 3.9 (The determinant does not use the loss)**.** Let A be the per-direction iteration matrix (15) (for either the EMA or Delta rule) with the coupling $\eta\kappa_i$ replaced by an arbitrary constant $c > 0$, read as η times the local curvature along u_i under whatever loss is being minimized. The forgetting factors β and $\tilde{\beta}_i = \beta - \eta\hat{\lambda}_i$ keep the meaning they carry in Theorem 3.8, since Lemma 3.7 fixes them from the momentum recursion alone and no loss enters them, so c carries everything the loss contributes. Then $\det A = \tilde{\beta}_i$ for AK-MOMENTUM and $\det A = \beta$ for EMA momentum, for every c and every step size α. Consequently the best per-direction rate attainable over step sizes falls from $\sqrt{\beta}$ to $\sqrt{\tilde{\beta}_i}$ on every direction with $c > 0$, whatever loss produced it.

The determinant is the same for every c, so it is the same for every loss that produces a positive coupling, and this is what carries Theorem 3.8 out of the squared-loss setting. Appendix I.1 proves the lemma and the rest of Appendix I uses it to extend the guarantee to the two settings named above. The proof uses only that the parameter error enters the buffer through some per-direction coupling and that the coupling cancels in the determinant. We state the conclusion over step sizes rather than

at a fixed one, because at a step size held fixed across the two methods a smaller determinant does not by itself force a smaller spectral radius.

We further prove in Theorem F.2 that, whenever the per-direction iteration is underdamped along u_i, this determinant reduction translates into a strictly smaller per-direction spectral radius. The underdamped condition reduces to a band condition on $\alpha\eta\kappa_i$ (Remark F.3). We defer the statement carrying that band condition to the appendix.

3.4 Non-stationary Tracking Dynamics

The fixed-point analysis of Section 3.1 and the linear-regression dynamics of Section 3.3 both assume stationarity. In practice, the population gradient $\bar{G}_t = \nabla_\theta \mathcal{L}(\theta_t)$ and the input-feature covariance $\Sigma_x(\theta_t) = \mathbb{E}[x_t x_t^\top]$ both drift continuously as the weights update. We now characterize the rate at which the momentum buffer adapts to such drift.

Theorem 3.10 (Direction-selective tracking under distribution shift)**.** *Suppose at step t_0 the population gradient and input-feature covariance shift to new fixed values $(\bar{G}_k, \Sigma_k)$, and let M^* be the corresponding new fixed point. Define the tracking error $T_{t,i} = (M_t - M^*)u_i$ along eigendirection u_i of Σ_k. Then*

$$\textit{EMA:} \quad \mathbb{E}[T_{t,i} \mid T_{t-1,i}] = \beta T_{t-1,i}, \quad \forall i, \tag{16}$$

$$\textit{Delta:} \quad \mathbb{E}[T_{t,i} \mid T_{t-1,i}] = \tilde{\beta}_i T_{t-1,i} = (\beta - \eta\lambda_i) T_{t-1,i}. \tag{17}$$

EMA contracts uniformly at rate β. AK-MOMENTUM *contracts along u_i at rate $\tilde{\beta}_i$, strictly faster for every direction with $\lambda_i > 0$.*

Theorem 3.10 follows immediately from Lemma 3.7, holds for any β and η in the stable range with no further restriction, and applies in expectation along every direction (proof in Appendix G). Unrolling (17) gives expected memory horizons of $\tau_i^{\mathrm{Delta}} = 1/((1-\beta) + \eta\lambda_i)$ along u_i versus $\tau_i^{\mathrm{EMA}} = 1/(1-\beta)$ uniformly, identical to (14), and shorter under AK-MOMENTUM by a factor of $1 + \eta\lambda_i/(1-\beta)$. Tighter direction-uniform bounds and density-weighted mean contraction rates are deferred to Appendix G.2.

Theorem 3.10 constrains the recursion that produces the buffer, specifically the operator $\beta I - \eta\hat{x}_t\hat{x}_t^\top$ of (7), and places no condition on the loss landscape. It is therefore the result that survives into non-convex training, and it sharpens into a lag bound there.

Proposition 3.11 (Steady lag under drift)**.** If the target of the buffer drifts by at most Δ_i per step along u_i, then $\limsup_t \|\mathbb{E}[T_{t,i}]\| \le \tilde{\beta}_i\Delta_i/(1-\tilde{\beta}_i)$, against $\beta\Delta_i/(1-\beta)$ for EMA. Since $\tilde{\beta}_i < \beta$ on every direction with positive input density and $t \mapsto t/(1-t)$ is increasing, the bound is strictly smaller there, and the relaxation-time ratio is $1 + \eta\hat{\lambda}_i/(1-\beta)$.

In the above proposition, convexity never enters, so this holds for the deep non-convex losses of Section 4. Appendix I.4 proves it, adds a companion bound that is uniform over directions when the drift follows the input density, and connects the reduced lag back to the first-order loss decrease of Proposition D.1. Lastly, we clarify that the above is a tracking result and does not give a global convergence rate on non-convex losses.

What gets forgotten, what gets preserved. AK-MOMENTUM couples input-direction density to gradient staleness. Along high-density directions (λ_i large), the local gradient changes rapidly with θ and the buffer overwrites stale content on a shorter horizon. Along low-density directions (λ_i small), the gradient is approximately stationary and is preserved on an EMA-like time scale. This is exactly the data-driven schedule the function-space prediction loss prescribes.

The results of this section carry different amounts of assumption, and Appendix H states which set of assumptions describes a training run.

4 Experiments

The theory of Section 3 gives three effects: implicit input-side preconditioning at the fixed point (Theorem 3.4), direction-density-aware memory transport (Lemma 3.7), and small constant FLOP

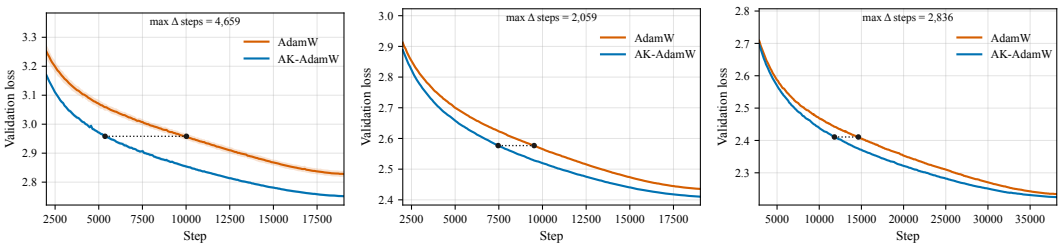

(a) 67M, 3 seeds, 10BT. (b) 370M, 3 seeds, 10BT. (c) 1B, 1 seed, 20BT.

Figure 1: Validation loss against optimizer step on FineWeb-Edu at 67M, 370M, and 1B parameters. The gain holds at every scale we ran, including the 1B Chinchilla-optimal run in (c). Curves at 67M and 370M are seed means with per-seed bands, and the 1B curve is a single seed. AK-AdamW separates from AdamW early and stays below it for the rest of training at all three scales. The annotation marks the largest step saving over matched validation-loss levels, in steps, measured from the seed-mean curve. Curves are cropped at the left to omit the early high-loss region, which compresses the later separation.

overhead (Theorem M.3). To test whether these claims hold in deep, non-linear, non-stationary training we run four sets of experiments. (a) We compare AK-AdamW against AdamW on Llama-2-style language-model pretraining at 67M, 370M, and 1B parameters on FineWeb-Edu (Section 4.1), isolating the contribution of AK-MOMENTUM. (b) We compare with a tuned Muon baseline under the same search protocol, as a reference point among structured optimizers, summarized in Section 4.1 and fully reported in Appendix O. (c) We probe the theoretical effects with a per-layer mechanistic diagnostic harness on the 67M run (Section 4.2). (d) We verify generality across optimizer families and architectures, comparing AK-SGD against SGD with EMA momentum on an MLP, and AK-AdamW against AdamW on ResNet-18 and ViT-Tiny, all on CIFAR-10 (Section 4.3). Full setup for every run, including architectures, data, tuning protocol, and compute, is in Appendix N.

4.1 Main Results: Validation Loss on FineWeb-Edu

Per-sample step efficiency. At all three scales AK-AdamW reaches AdamW's validation loss in substantially fewer steps and continues to a lower terminal value (Figure 1). The two curves separate shortly after warmup and do not cross again at any scale, so AK-AdamW is below AdamW at every matched step over the entire training horizon. Table 2 reports the paired gap against AdamW across matched validation-loss levels. The sign of the paired gap is the same in every run at every scale, and at 370M the mean gap is 13.7 times its seed standard deviation. Every hyperparameter at 370M and 1B is carried over from the 67M sweep with no re-tuning, under the μP rule of Theorem Q.1. The two branches share initialization, data order, and schedule at each scale. The advantage is evident early and persists through the cosine decay, which is what Theorem 3.10 and Proposition 3.11 predict for a drifting target without assuming convexity or stationarity (Appendix H). Section 4.2 measures the mechanism directly.

Table 2: AK-AdamW against AdamW on FineWeb-Edu across matched validation-loss levels. Loss gap is in nats and step reduction is the fraction of AdamW steps saved to reach the same loss, both reported as mean and maximum over the matched levels with the seed standard deviation. The 1B scale run was done on a single seed and uses the Chinchilla-optimal token budget at that size, with the cosine cycle stretched and warmup steps held fixed, identically for both optimizers. Matched levels are taken over the range plotted in Figure 1. Detailed settings are stated in Appendix N.

Scale (seeds, tokens)	Mean loss gap	Max loss gap	Mean step red.	Max step red.
67M (3 seeds, 10BT)	0.0936 ± 0.0150	0.1077 ± 0.0146	$39.25 \pm 4.55\%$	$46.39 \pm 4.32\%$
370M (3 seeds, 10BT)	0.0383 ± 0.0028	0.0501 ± 0.0016	$17.61 \pm 0.95\%$	$22.12 \pm 0.80\%$
1B (1 seed, 20BT)	0.0245	0.0361	13.43%	19.37%

Per-FLOP compute efficiency. Table 3 collects the cost side of the comparison, and Figure 4 plots the same runs against wall clock. The realized per-step overhead of the deployed rule is 11.2% at

67M and 17.4% at 370M, counted over the actual runs, and it rises with width toward the band of Theorem M.3 as the linear layers take a larger share of the step. Measured end-to-end step time on a single H200 is $1.177\times$ AdamW at 67M and $1.153\times$ at 370M. Section M.6 gives the counted overhead at all three scales. Unlike the per-step comparison, the cost axes have a crossing point, which occurs early at 420 PFLOPs of the 4.0 EFLOP horizon at 67M and at 5.10 EFLOPs of the 22.2 EFLOP horizon at 370M, which is about a tenth and about a quarter of the way through the respective runs, and past that point it is ahead on executed FLOPs and on wall clock at both scales.

Table 3: A cost table for the deployed algorithm. Overhead is the realized per-step FLOP overhead counted over the actual runs, step time is measured end to end on a single H200, and the savings are averaged over the matched validation-loss levels past the crossing point, with the best matched level in parentheses. Appendix M gives the full count and the measurement setup. We report the cost comparison at the two scales for which we ran the full matched-loss measurement.

Scale	FLOP overhead	Step time	FLOPs saved	Wall clock saved
67M	11.2%	$1.177\times$	25.9% (32.6%)	21.6% (28.7%)
370M	17.4%	$1.153\times$	4.5% (9.4%)	6.2% (11.0%)

A reference point comparison among structured optimizers. AdamW is the baseline that isolates the contribution of AK-MOMENTUM. We add a tuned Muon baseline as a reference point among optimizers that address anisotropy at a different place within the optimizer, by post-processing the buffer rather than changing how it is formed. The baseline was tuned under the same Optuna protocol, and ran with 3 seeds at each of 67M and 370M. The validation loss curve of AK-AdamW sits below Muon at both scales, with a mean loss gap of 0.120 ± 0.008 nats at 67M and 0.109 ± 0.003 at 370M, and the sign is consistent in every run. Muon received the largest per-dimension search budget among all three arms and was tuned under its own μP rule [19] rather than an Adam-family rule [29]. We make no general claim about Muon from this, and we report it as a baseline tuned inside our protocol. Full tables, curves, protocol, and the scope of the comparison are in Appendix O.

4.2 Mechanistic Diagnostics: Validating the Theoretical Picture

Section 3 predicts three quantities that should differ between EMA momentum and AK-MOMENTUM: the buffer's alignment with the population gradient (Section 4.2.1), its function-space prediction error on output-side errors (Section 4.2.2), and the conditioning of the input-feature covariance (Section 4.2.3). These sit at three points of one mechanism. Section 4.2.2 measures the loss whose minimization defines AK-MOMENTUM and its input-side preconditioning, Section 4.2.1 measures the buffer in the role that by Proposition D.1 governs per-step loss decrease, and Section 4.2.3 measures the input-feature covariance that the preconditioning acts on. We probe each at fixed evaluation steps on the 67M run with a per-layer diagnostic harness on a held-out probe batch.

4.2.1 Improved Gradient-Estimator Quality

We measure the momentum–gradient cosine and the relative prediction error between the pre-step buffer M_t and current gradient g_t, on global parameters (definitions, pre-step semantics, and sign convention are explained in Appendix P.1). Figure 2(a,b) shows AK-AdamW maintains *strictly higher* cosine and *steadily lower* relative prediction error e_t than AdamW at every logged step, consistent with Section 3.1's gradient-estimator interpretation.

4.2.2 Function-Space Prediction Error

The function-space view of Definition 3.3 predicts that AK-MOMENTUM's update rule explicitly performs online stochastic gradient descent on the prediction loss $\frac{1}{2}\|\delta - M\hat{x}\|^2$, so its buffer should be a better predictor of the output-side error δ given the input $\hat{x}$ than EMA, which is not optimizing this loss at all. To test this directly, at each evaluation checkpoint we freeze the buffer M_t for both optimizers, sample a held-out probe batch, compute the predicted output-side error $\widehat{\delta}_t = M_t\hat{x}_t$ per layer, and compare against the true δ_t. Figure 2c reports the cosine similarity $\cos(\widehat{\delta}, \delta)$.

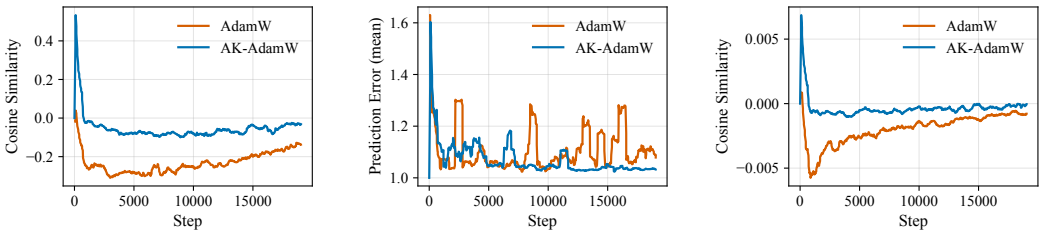

(a) Momentum–gradient cosine similarity.

(b) Momentum–gradient prediction error.

(c) Gradient–prediction cosine similarity.

Figure 2: Mechanistic diagnostics on momentum buffer on the 67M run. At every logged step, AK-AdamW (blue) maintains **(a)** higher $\cos(M_t, g_t)$, **(b)** lower $e_t = \|M_t - g_t\|_F / \|g_t\|_F$, and **(c)** higher $\cos(M_t \hat{x},\ \delta)$ than AdamW (orange). Negative values are an artifact of stochastic descent itself, not the buffer rule, and apply equally to both optimizers. The diagnostic quantity is the gap, uniformly favorable to AK-AdamW.

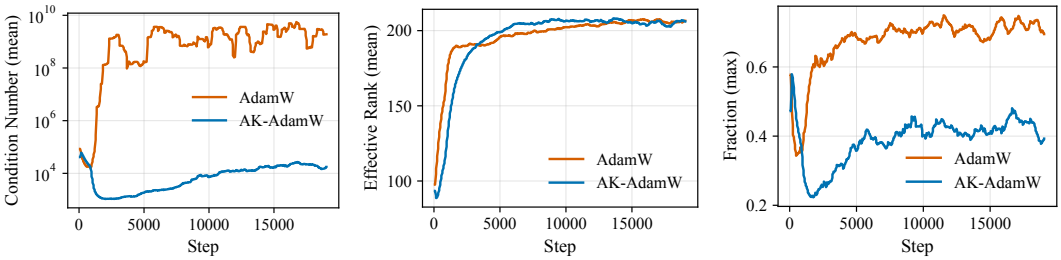

(a) Condition number (mean).

(b) Effective rank (layerwise mean).

(c) Top-1 variance fraction (max).

Figure 3: Input-feature covariance diagnostics on the 67M run. Across all three statistics, layers trained with AK-AdamW (blue) maintain healthier feature spectra than those trained with AdamW (orange), consistent with the implicit input-side preconditioning predicted by Theorem 3.4.

4.2.3 Robustness Against Anisotropic Collapse of Input Features

Theorem 3.4 predicts that AK-MOMENTUM implements implicit input-side preconditioning. Along an eigendirection u_i of the input-feature covariance with directional density λ_i, the steady-state buffer is scaled by $\phi_i = 1/(\mu + \lambda_i)$ rather than by 1 as in EMA, which actively counteracts the dominance of high-density directions. If this mechanism is operating during training, then the input-feature covariance of layers under AK-AdamW should remain better-conditioned (lower condition number, higher effective rank, lower top-1 variance fraction) than under AdamW. We compute three statistics of the per-layer input-feature covariance: the layerwise mean of the condition number $\lambda_{\max}/\lambda_{\min}$ and the effective rank $\exp(H(\boldsymbol{\lambda}/\sum \lambda_i))$ where H is Shannon entropy, and the maximum top-1 variance fraction $\lambda_{\max}/\sum \lambda_i$. Figure 3 summarizes the result. Feature covariances under AK-AdamW remain meaningfully better-conditioned than those under AdamW, with consistently lower condition number, higher effective rank, and lower top-1 variance fraction throughout training. These are also the measurements that separate the delta correction from the diagonal second moment of AdamW, which accumulates $g^{\odot 2}$ and therefore registers only the per-coordinate input energies $\mathbb{E}[x_k^2]$, the diagonal of Σ_x, and never its off-diagonal correlations or eigendirections, and Appendix K discusses that interaction.

Interpretation. All three diagnostics move in the direction Section 3 predicts, with consistent magnitudes.

4.3 Generality Across Optimizer Families and Architectures

To verify that the gain transfers beyond Adam's diagonal preconditioner, we compare AK-SGD with SGD-momentum on a 3-hidden-layer MLP on CIFAR-10. AK-SGD reaches SGD's validation loss earlier and converges to a strictly lower terminal value, with the gap opening right after the first epoch and persisting throughout. Validation curves and test accuracy are in Appendix R.

To verify that it also transfers beyond language modeling and beyond a single architecture, we run ResNet-18 and ViT-Tiny on CIFAR-10 for 120 epochs, AK-AdamW against AdamW with 3 seeds and an identical log-scale learning-rate sweep for each optimizer. Table 4 reports the training-loss gap at matched epochs, averaged over the phase where the curves separate, and the sign of the gap is the same in all runs. Appendix R.1 gives the curves, the averaging window, and why each architecture is read on the curve that measures optimization rather than the inductive bias of the model. We read this as a generality check rather than a second pillar of evidence, and language-model pretraining remains where the claims of this paper are made.

Table 4: AK-AdamW against AdamW on CIFAR-10 over 120 epochs with 3 seeds. Gaps are training loss at matched epochs, in nats and relative to the AdamW loss at that epoch, averaged over the phase where the curves separate. We report training loss for both architectures here so the two rows are on the same footing, and Appendix R.1 gives the validation-loss curve for ResNet-18. Curves are in Appendix R.

Architecture	Mean gap (nats)	Mean gap (%)	Max gap (nats)	Max gap (%)
ViT-Tiny	0.079 ± 0.013	25.1 ± 2.7	0.140 ± 0.017	45.5 ± 3.5
ResNet-18	0.041 ± 0.006	11.1 ± 1.6	0.081 ± 0.016	15.1 ± 1.8

5 Conclusion

AK-MOMENTUM replaces the EMA accumulator with the classical delta rule, treating the first-moment buffer as an online linear associative memory of the factored gradient $\delta_t x_t^\top$. The anisotropic memory transport mechanism (Lemma 3.7) unifies its steady-state, per-direction convergence, and non-stationary behavior. AK-AdamW reduces steps-to-target loss by up to $46.39 \pm 4.32\%$ at 67M and $22.12 \pm 0.80\%$ at 370M on FineWeb-Edu, the gain holds at 1B on a Chinchilla-optimal budget, and AK-SGD, ResNet-18, and ViT-Tiny show the same pattern on CIFAR-10.

Limitations and Future Work. Experiments cover language modeling up to 1B parameters and CIFAR-10 classifiers, so larger scale and non-language generative domains such as image generation and reinforcement learning remain open. On implementation, the deployed rule is $M \leftarrow \beta M + \eta(G - M\hat{\Sigma})$ and its counted per-step cost rises with width, reaching 20.3% at 1B, with the per-layer share varying with layer shape as Appendix M sets out. Reported wall-clock numbers use a non-fused implementation, and a fused backward and optimizer kernel would narrow the gap to the count. Our two modalities are trained separately rather than interleaved, and a run that mixes them is the natural next step, with Appendix J setting out why the analysis already covers mixed input types. Buffer-level compositions with Muon, Shampoo, and SOAP remain future work, and each deserves its own controlled study. A controlled comparison against a gradient-keyed delta rule on the buffer [3], which isolates the choice of key, is left to future work as well.

Acknowledgments and Disclosure of Funding

This work is supported by NSF Grants 2339112, 2512805, Jane Street, and Pennsylvania Infrastructure Technology Alliance.

References

[1] Takuya Akiba, Shotaro Sano, Toshihiko Yanase, Takeru Ohta, and Masanori Koyama. Optuna: A next-generation hyperparameter optimization framework. In *Proceedings of the 25th ACM SIGKDD international conference on knowledge discovery & data mining*, pages 2623–2631, 2019.

[2] Ali Behrouz, Meisam Razaviyayn, Peilin Zhong, and Vahab Mirrokni. It's all connected: A journey through test-time memorization, attentional bias, retention, and online optimization. *arXiv preprint arXiv:2504.13173*, 2025.

[3] Ali Behrouz, Meisam Razaviyayn, Peilin Zhong, and Vahab Mirrokni. Nested learning: The illusion of deep learning architectures. *Advances in Neural Information Processing Systems*, 38: 46968–47002, 2025. Extended version: arXiv:2512.24695.

[4] Ashok Cutkosky and Francesco Orabona. Momentum-based variance reduction in non-convex SGD. In *Advances in Neural Information Processing Systems*, volume 32, pages 15236–15245, 2019.

[5] Zhehang Du and Weijie Su. The Newton-Muon optimizer. *arXiv preprint arXiv:2604.01472*, 2026.

[6] Kawin Ethayarajh. How contextual are contextualized word representations? comparing the geometry of bert, elmo, and gpt-2 embeddings. In *Proceedings of the 2019 conference on empirical methods in natural language processing and the 9th international joint conference on natural language processing (EMNLP-IJCNLP)*, pages 55–65, 2019.

[7] Behrooz Ghorbani, Shankar Krishnan, and Ying Xiao. An investigation into neural net optimization via hessian eigenvalue density. In *International Conference on Machine Learning*, pages 2232–2241. PMLR, 2019.

[8] Vineet Gupta, Tomer Koren, and Yoram Singer. Shampoo: Preconditioned stochastic tensor optimization. In *International Conference on Machine Learning*, pages 1842–1850. PMLR, 2018.

[9] Keller Jordan, Yuchen Jin, Vlado Boza, Jiacheng You, Franz Cesista, Laker Newhouse, and Jeremy Bernstein. Muon: An optimizer for hidden layers in neural networks. `https://kellerjordan.github.io/posts/muon/`, 2024.

[10] Diederik P Kingma and Jimmy Ba. Adam: A method for stochastic optimization. *arXiv preprint arXiv:1412.6980*, 2014.

[11] Alex Krizhevsky. Learning multiple layers of features from tiny images. Technical report, University of Toronto, Toronto, ON, Canada, 2009.

[12] Ilya Loshchilov and Frank Hutter. Decoupled weight decay regularization. *arXiv preprint arXiv:1711.05101*, 2017.

[13] James Martens and Roger Grosse. Optimizing neural networks with kronecker-factored approximate curvature. In *International conference on machine learning*, pages 2408–2417. PMLR, 2015.

[14] Jiaqi Mu, Suma Bhat, and Pramod Viswanath. All-but-the-top: Simple and effective postprocessing for word representations. *arXiv preprint arXiv:1702.01417*, 2017.

[15] Yurii Nesterov. A method for solving the convex programming problem with convergence rate $o(1/k^2)$. *Doklady Akademii Nauk SSSR*, 269(3):543–547, 1983.

[16] Vardan Papyan. Measurements of three-level hierarchical structure in the outliers in the spectrum of deepnet hessians. *arXiv preprint arXiv:1901.08244*, 2019.

[17] Guilherme Penedo, Hynek Kydlíček, Anton Lozhkov, Margaret Mitchell, Colin Raffel, Leandro Von Werra, Thomas Wolf, et al. The fineweb datasets: Decanting the web for the finest text data at scale. *Advances in Neural Information Processing Systems*, 37:30811–30849, 2024.

[18] Boris T Polyak. Some methods of speeding up the convergence of iteration methods. *Ussr computational mathematics and mathematical physics*, 4(5):1–17, 1964.

[19] Shikai Qiu, Zixi Chen, Hoang Phan, Qi Lei, and Andrew Gordon Wilson. Hyperparameter transfer enables consistent gains of matrix-preconditioned optimizers across scales. In *Advances in Neural Information Processing Systems*, 2025.

[20] Levent Sagun, Utku Evci, V Ugur Guney, Yann Dauphin, and Leon Bottou. Empirical analysis of the hessian of over-parametrized neural networks. *arXiv preprint arXiv:1706.04454*, 2017.

[21] Imanol Schlag, Kazuki Irie, and Jürgen Schmidhuber. Linear transformers are secretly fast weight programmers. In *International conference on machine learning*, pages 9355–9366. PMLR, 2021.

[22] Noam Shazeer and Mitchell Stern. Adafactor: Adaptive learning rates with sublinear memory cost. In *International conference on machine learning*, pages 4596–4604. PMLR, 2018.

[23] Ilya Sutskever, James Martens, George Dahl, and Geoffrey Hinton. On the importance of initialization and momentum in deep learning. In *International conference on machine learning*, pages 1139–1147. pmlr, 2013.

[24] Hugo Touvron, Louis Martin, Kevin Stone, Peter Albert, Amjad Almahairi, Yasmine Babaei, Nikolay Bashlykov, Soumya Batra, Prajjwal Bhargava, Shruti Bhosale, et al. Llama 2: Open foundation and fine-tuned chat models. *arXiv preprint arXiv:2307.09288*, 2023.

[25] Nikhil Vyas, Depen Morwani, Rosie Zhao, Mujin Kwun, Itai Shapira, David Brandfonbrener, Lucas Janson, and Sham Kakade. Soap: Improving and stabilizing shampoo using adam. *arXiv preprint arXiv:2409.11321*, 2024.

[26] Zhengbo Wang, Jian Liang, Ran He, Zilei Wang, and Tieniu Tan. Taming momentum: Rethinking optimizer states through low-rank approximation. In *International Conference on Learning Representations*, 2026.

[27] Bernard Widrow and Marcian E Hoff. Adaptive switching circuits. In James A. Anderson and Edward Rosenfeld, editors, *Neurocomputing: Foundations of Research*, pages 123–134. MIT Press, 1988. Reprinted from *1960 IRE WESCON Convention Record*, Part 4, pp. 96–104.

[28] Yangyang Xu and Yibo Xu. Momentum-based variance-reduced proximal stochastic gradient method for composite nonconvex stochastic optimization. *Journal of Optimization Theory and Applications*, 196(1):266–297, 2023.

[29] Ge Yang, Edward Hu, Igor Babuschkin, Szymon Sidor, Xiaodong Liu, David Farhi, Nick Ryder, Jakub Pachocki, Weizhu Chen, and Jianfeng Gao. Tuning large neural networks via zero-shot hyperparameter transfer. *Advances in Neural Information Processing Systems*, 34:17084–17097, 2021.

[30] Songlin Yang, Bailin Wang, Yu Zhang, Yikang Shen, and Yoon Kim. Parallelizing linear transformers with the delta rule over sequence length. *Advances in neural information processing systems*, 37:115491–115522, 2024.

[31] Thomas T. Zhang, Alok Shah, Yifei Zhang, Vincent Zhang, Nikolai Matni, and Max Simchowitz. Double preconditioning (DoPr): Optimization for test-time performance, not validation loss. *arXiv preprint arXiv:2606.06418*, 2026.

A Symbols and Notation

Table 5: Notation used in the analysis. The left block is the unnormalized-key reading and the right block is the normalized-key reading, which is the deployed algorithm.

Symbol	Meaning	Where it enters
$x,\ \delta$	input activation, output-side error $\partial\mathcal{L}/\partial y$	key and value of the association
$\hat{x} = x/\|x\|_2$	normalized key	deployed update
$X, \hat{X}, \Delta$	batched inputs, normalized inputs, errors	Appendix M
$\Sigma_x = \mathbb{E}[xx^\top]$	input covariance	unnormalized analysis
$\hat{\Sigma} = \mathbb{E}[\hat{x}\hat{x}^\top]$	key second moment, $\operatorname{tr}\hat{\Sigma} = 1$	deployed analysis
$\lambda_i,\ \hat{\lambda}_i,\ u_i$	eigenvalues of Σ_x, of $\hat{\Sigma}$, shared eigenvectors	per-direction statements
$\kappa_i = u_i^\top \mathbb{E}[\|x\|\,\hat{x}\hat{x}^\top]u_i$	per-direction gradient coupling	trace of (15)
$\bar{G} = \mathbb{E}[\delta x^\top],\ \hat{G} = \mathbb{E}[\delta\hat{x}^\top]$	mean gradient in raw and normalized keys	fixed points
G	batch estimate of $\hat{G}$	deployed update
$M,\ M^*$	momentum buffer and its fixed point	Theorem 3.4
$\beta,\ \eta$	EMA decay, delta-rule coefficient	(6)
$\tilde{\beta}_i = \beta - \eta\hat{\lambda}_i$	per-direction memory contraction	Lemma 3.7
$\mu = (1-\beta)/\eta$	Tikhonov ridge	Theorem 3.4
$\tau_i = 1/((1-\beta) + \eta\hat{\lambda}_i)$	per-direction memory horizon	(14)
$r_i = \eta\hat{\lambda}_i/(1-\beta)$	forgetting speed-up over EMA	Appendix I
$m,\ n,\ N,\ \gamma$	output width, input width, tokens per step, gated-MLP ratio	Appendix M

B Extended Related Work

Momentum and acceleration. First-moment EMA momentum has been a near-universal component of deep-network optimizers since heavy-ball momentum [18], which is the source of the view of the buffer as inertia. A separate line starting from Nesterov's accelerated gradient [15] builds accelerated methods on a lookahead rather than on the EMA first moment used in SGD-momentum and Adam-style optimizers, so we place it here rather than on the buffer itself. The empirical importance of momentum in neural-network training was established by Sutskever et al. [23], together with its interaction with initialization and with momentum schedules. The reading of the buffer as gradient denoising is developed directly in the smoothing and variance-reduction line [4, 28]. The isotropic, scalar-decay form of EMA has been retained in essentially every adaptive optimizer derived from Adam [10, 12]. AK-MOMENTUM departs from this lineage by replacing the EMA update itself with a delta-rule update on a function-space prediction loss, keyed on the input activation. The delta-rule constructions of Behrouz et al. [3] depart from the same lineage, on a loss keyed on the gradient instead.

Online associative memory and the delta rule. The delta rule [27] is the canonical online stochastic gradient method for linear least squares with key–value targets. In recent deep-learning literature, the delta rule has reappeared as the backbone of linear-attention fast-weight programmers [21, 30], where a memory matrix stores key–value associations across a sequence and is updated online to minimize retrieval error. AK-MOMENTUM imports this online-associative-memory machinery into the optimizer, so the first-moment buffer plays the role of the memory matrix, the layer's input activations and output-side errors play the roles of keys and values, and the per-step update is exactly the regularized delta rule. The view of the optimizer and its momentum as an associative memory over gradients has also appeared in Behrouz et al. [2, 3]. They factor the layer gradient into an outer product of the input activation and a local error and carry that reading to the momentum term, writing the momentum as an associative memory whose objective is a free design choice rather than a fixed one. They then instantiate that choice with a delta rule keyed on the gradient. They also give a delta rule that does key on the input activation, but it replaces the descent step on the weights rather than the momentum buffer. This paper newly devises the activation-keyed instantiation of the momentum objective and the theory that it supports. What the choice of objective decides is the form of the resulting rule. The dot-product objective $\langle Mx, \delta\rangle$ has gradient step $\delta x^\top$, so it returns the Hebbian

accumulator of Section 2.2, which is EMA momentum with its single decay rate. The function-space prediction loss of Definition 3.3, on the same key and value, produces the state-dependent forgetting factor of (7) instead. Table 6 places the three rules side by side.

Table 6: Where the delta rule is applied and what keys it. The first two rows are the constructions of Behrouz et al. [3], written throughout in the notation of Table 5, so β and η denote the decay and the step size belonging to the rule in that row rather than a value shared across rows. The forgetting factor right-multiplies the object in the second column. Of the two buffer-level rules, only the activation-keyed one has a forgetting factor whose expectation is $\beta I - \eta\Sigma_x$, the matrix Lemma 3.7 and everything downstream of it act on.

Rule	Applied to	Key	Value	Forgetting factor
Weight-level [3]	weights W	input activation x	output-side error δ	$I - \eta\, xx^\top$
Buffer-level [3]	momentum M	gradient g	preconditioner	$\beta I - g^\top g$
AK-MOMENTUM (ours)	momentum M	normalized input activation $\hat{x}$	output-side error δ	$\beta I - \eta\, \hat{x}\hat{x}^\top$

Anisotropy in deep-network optimization. The anisotropy of the deep-network loss landscape has been documented extensively. Hessian-eigenvalue-density studies [20, 7, 16] report a small bulk of large eigenvalues followed by a long, near-flat tail spanning several orders of magnitude. Activation-anisotropy studies in NLP [14, 6] show that learned representations concentrate disproportionately along a handful of dominant directions. These findings have motivated optimizers that explicitly account for anisotropy. K-FAC [13] approximates the Fisher information by Kronecker-factored input/output curvature. Shampoo [8] applies Kronecker-factored preconditioning to the gradient. SOAP [25] refines the eigenbasis used by Shampoo. Muon [9] applies Newton–Schulz orthogonalization to the EMA momentum to flatten its singular-value spectrum. Adafactor [22] factorizes the second-moment statistics. A unifying property of these methods is that they retain the EMA momentum update and apply external structural processing (preconditioning before, post-conditioning after) to address anisotropy. AK-MOMENTUM addresses anisotropy at a different level of the optimizer stack, inside the momentum update itself. Therefore, AK-MOMENTUM is complementary to, rather than in competition with, these methods.

Concurrent work on activation-side preconditioning. Concurrent with this work, DoPr [31] pairs a gradient-based preconditioner such as Adam or Muon with an activation-based preconditioner in the style of K-FAC, on the argument that non-isotropic input activations degrade feature learning. The object it adds is the input-side Kronecker factor, chosen over the full K-FAC preconditioner to avoid the output-side factor and the extra optimizer state it needs. That is the factor Theorem 3.4 shows AK-MOMENTUM reaches implicitly, without inversion, damping, or state beyond the momentum the base optimizer already keeps. Newton-Muon [5] reaches the same factor from a different direction. It approximates the layer loss by a quadratic surrogate in the gradient, an output-side curvature matrix, and the matrix of input activations, and minimizing that surrogate right-preconditions the gradient by the inverse input second moment before the usual Muon pipeline. It reads standard Muon as a Newton-type method that drops this right preconditioner. Both methods differ from ours in level, since each forms an explicit preconditioner and applies it to a buffer that is still an EMA, while AK-MOMENTUM changes the buffer itself, so they compose with it rather than substitute for it. DoPr reports downstream test-time performance under rollout and Newton-Muon reports iterations to a target validation loss on a GPT-2 speedrun configuration, so neither set of results is directly comparable with ours.

AK-AdamW vs. AdamW is a controlled head-to-head that isolates the first-moment update. The empirical contribution of this paper is the delta-rule update applied to the first-moment buffer, and cleanly isolating that contribution requires a baseline that differs from AK-AdamW *only* in the first-moment update. AdamW is the unique such baseline. The second moment, bias correction, and decoupled weight decay are identical between AK-AdamW and AdamW, and setting the state-dependent forgetting factor of (7) to zero returns (1) exactly, so AdamW is the null case of the mechanism and any difference in the loss curve is attributable to the EMA-vs-delta swap. Any other delta-rule buffer, including one keyed on the gradient, differs from AK-AdamW in the choice of key rather than in whether the mechanism is present, so it isolates a different variable. Head-to-heads against Muon, Shampoo, or SOAP would conflate the first-moment contribution with Newton–Schulz

orthogonalization or with Kronecker-factored preconditioning applied at a different level of the optimizer stack, which is precisely the level at which those methods address anisotropy and at which AK-MOMENTUM is complementary, not substitutive. The natural compositions, AK-MUON, AK-SHAMPOO, and AK-SOAP, inherit AK-MOMENTUM's first-moment update while retaining the structural processing of the base optimizer, and we identify them as future work in Section 5, and an isolated AK-AdamW vs. AdamW comparison is the prerequisite for those follow-ups, not a substitute for them. The AK-SGD vs. SGD-momentum result on CIFAR-10 (Section 4.3) provides a parallel controlled comparison in the family without an adaptive denominator, verifying that the gain is attributable to the delta-rule mechanism rather than to its interaction with Adam's diagonal preconditioner.

C Stability of the Normalized-key AK-MOMENTUM

The normalized-key variant gives input-scale-independent contraction under a width-independent condition $\eta < \beta$, unlike the unnormalized-key variant. This is the main practical reason for deploying it in deep-network training.

Proposition C.1 (Bounded directional second moment)**.** Let $x \in \mathbb{R}^n$ be any random vector with $\Pr(\|x\| > 0) = 1$, and let $\hat{x} = x/\|x\|$. Then $\hat{\Sigma} := \mathbb{E}[\hat{x}\hat{x}^\top]$ satisfies

$$\operatorname{tr}(\hat{\Sigma}) = 1 \qquad \text{and} \qquad 0 \le \hat{\lambda}_i \le 1 \text{ for all } i, \tag{18}$$

with $\sum_i \hat{\lambda}_i = 1$.

Proof. $\operatorname{tr}(\hat{\Sigma}) = \mathbb{E}[\operatorname{tr}(\hat{x}\hat{x}^\top)] = \mathbb{E}[\hat{x}^\top \hat{x}] = \mathbb{E}[\|\hat{x}\|^2] = 1$. Each eigenvalue is non-negative since $\hat{\Sigma}$ is positive semi-definite, and bounded above by the trace. □

Normalized-key variant. $\hat{x}_t := x_t/\|x_t\|$, giving

$$M_t = \beta M_{t-1} + \eta(\delta_t - M_{t-1}\hat{x}_t)\hat{x}_t^\top. \tag{19}$$

Theorem C.2 (Input-scale-independent contraction of the normalized variant)**.** *The normalized-key* AK-MOMENTUM *recurrence* (19) *contracts in expectation along every input direction whenever $\eta < \beta$,* independent of *input scale, layer index, or training step. In contrast, the original unnormalized-key* AK-MOMENTUM (6) *requires the input-dependent and time-varying condition $\eta < \beta/\lambda_{\max}(\Sigma_x)$.*

Proof. By Lemma 3.7, the expected per-direction memory contraction along the eigendirection $\hat{u}_i$ of $\hat{\Sigma}$ is $\tilde{\beta}_i = \beta - \eta\hat{\lambda}_i$. By Proposition C.1, $\hat{\lambda}_i \le 1$, hence $\tilde{\beta}_i \ge \beta - \eta > 0$ under the stated condition, so the buffer contracts along every direction in expectation. For the unnormalized variant the contraction along eigenvector u_i of Σ_x is $\beta - \eta\lambda_i(\Sigma_x)$, which requires $\eta < \beta/\lambda_{\max}(\Sigma_x)$ and depends on input scale. □

The decoupling of η from input scale is the main practical reason for using the normalized variant in deep-network training, where activation scales vary by orders of magnitude across layers and through training.

Remark C.3 (Why normalization)**.** The forgetting operator is $\beta I - \eta\,\hat{x}_t\hat{x}_t^\top$, and its rank-one part has spectral norm $\|\hat{x}_t\hat{x}_t^\top\|_{\mathrm{op}} = 1$ at every width. This decouples η from width, since stability requires only $\eta < 1 + \beta$ and $\eta = \mathcal{O}(1)$ is admissible across all model widths. Without normalization, $\|x_t x_t^\top\|_{\mathrm{op}} \sim n$, forcing $\eta = \mathcal{O}(1/n)$. This is the foundation of μP-clean width transfer for AK-MOMENTUM.

D Why the Momentum Buffer Is Necessarily a Gradient Estimator

Proposition D.1 (First-order optimal momentum)**.** Let $\mathcal{L}$ be twice differentiable at θ_t with Hessian H_t. For any choice of M_t, the update $\theta_{t+1} = \theta_t - \alpha M_t$ satisfies

$$\mathcal{L}(\theta_{t+1}) = \mathcal{L}(\theta_t) - \alpha\,\langle M_t, \bar{G}(\theta_t)\rangle_F + \frac{\alpha^2}{2}\,\operatorname{tr}\big(M_t^\top H_t M_t\big) + O(\alpha^3), \tag{20}$$

where $\bar{G}(\theta_t) = \nabla_\theta \mathcal{L}(\theta_t)$. To first order in α, the loss decrease $\mathcal{L}(\theta_t) - \mathcal{L}(\theta_{t+1})$ is maximized over M_t of fixed Frobenius norm $\|M_t\|_F$ at $M_t \propto \bar{G}(\theta_t)$.

Proof. Equation (20) is the second-order Taylor expansion of $\mathcal{L}$ at θ_t with displacement $\Delta\theta = -\alpha M_t$. It holds pointwise for any realization of M_t, and no probabilistic averaging is required. The first-order term $-\alpha\langle M_t, \bar{G}(\theta_t)\rangle_F$ is linear in M_t, and by Cauchy–Schwarz $\langle M_t, \bar{G}_t\rangle_F$ is maximized over M_t of fixed Frobenius norm by alignment $M_t \propto \bar{G}_t$. □

Proposition D.1 is a Taylor identity, not a probabilistic assumption, since any realized buffer M_t that deviates from $\bar{G}(\theta_t)$ pays a first-order shortfall

$$\Delta_{\text{shortfall}} = \alpha\,\langle \bar{G}_t - M_t,\, \bar{G}_t\rangle_F \;\geq\; 0 \quad \text{(for fixed } \|M_t\|_F = \|\bar{G}_t\|_F\text{)}, \tag{21}$$

in the realized loss decrease relative to the optimal direction $M_t = \bar{G}_t$. The quality of M_t as an estimator of $\bar{G}_t$ therefore directly governs optimization efficiency. What differentiates between EMA and AK-MOMENTUM is the loss function on which the buffer performs online stochastic gradient descent.

E Proofs for Estimation Objectives and Fixed Point Analysis

E.1 Divergent optima

Proof. Weight-space.

$J_w(M) = \frac{1}{2}\|M\|_F^2 - \langle M, \bar{G}\rangle_F + \frac{1}{2}\mathbb{E}[\|\delta x^\top\|_F^2]$, $\nabla_M J_w = M - \bar{G} = 0 \Rightarrow M_w^* = \bar{G}$.

Function-space.

$J_f(M) = \frac{1}{2}\mathbb{E}[\|\delta\|^2] - \operatorname{tr}(M^\top\bar{G}) + \frac{1}{2}\operatorname{tr}(M\Sigma_x M^\top)$, where $\mathbb{E}[\delta^\top M x] = \operatorname{tr}(M^\top\bar{G})$ and $\mathbb{E}[x^\top M^\top M x] = \operatorname{tr}(M\Sigma_x M^\top)$, $\nabla_M J_f = -\bar{G} + M\Sigma_x = 0 \Rightarrow M_f^* = \bar{G}\,\Sigma_x^{-1}$. □

E.2 Update rules as online SGD

Proof. (a) $\nabla_M \ell_t^w = M - g_t$, so one SGD step with step α' gives $M \leftarrow M - \alpha'(M - g_t) = (1-\alpha')M + \alpha' g_t$. Setting $\alpha' = 1 - \beta$ recovers EMA. *(b)* $\nabla_M \ell_t^f = -(\delta_t - Mx_t)x_t^\top$, so one SGD step with step η gives $M \leftarrow M + \eta(\delta_t - Mx_t)x_t^\top$. At stationarity, $\mathbb{E}[\nabla_M \ell_t^f] = -(\bar{G} - M\Sigma_x) = 0 \Rightarrow M^* = \bar{G}\,\Sigma_x^{-1}$. □

E.3 Fixed Point Convergence of AK-MOMENTUM

Proof. Take expectations of (7) conditional on M_{t-1}: $\mathbb{E}[M_t \mid M_{t-1}] = M_{t-1}(\beta I - \eta\Sigma_x) + \eta\bar{G}$. At stationarity $M^* = M^*(\beta I - \eta\Sigma_x) + \eta\bar{G}$, hence $M^*[(1-\beta)I + \eta\Sigma_x] = \eta\bar{G}$ and (9). Projection onto u_i gives (10). □

E.4 Memory-theoretic reading

Theorem 3.4 can be read directly off Lemma 3.7: along u_i, the steady-state ratio of injection to forgetting is $\eta/[(1-\beta) + \eta\lambda_i] = \eta\tau_i$, the product of per-query injection gain η and direction-dependent memory horizon τ_i. Directions queried more often have shorter memory horizons, which reduces the steady-state retained mass along those directions, and this down-weighting *is* input-side whitening.

Remark E.1 (K-FAC connection)**.** The K-FAC approximation of the Fisher information for a linear layer is $F \approx \mathbb{E}[\delta\delta^\top] \otimes \mathbb{E}[xx^\top]$, with natural-gradient update $\mathbb{E}[\delta\delta^\top]^{-1}\,\bar{G}\,\Sigma_x^{-1}$. The pure delta-rule fixed point $\bar{G}\,\Sigma_x^{-1}$ is exactly the input-side factor of this Kronecker product. AK-MOMENTUM thus performs implicit input-side natural-gradient preconditioning without explicitly computing or inverting Σ_x, and the regularization parameter μ provides a numerically stable interpolation toward this preconditioner. As in Remark 3.6, the deployed algorithm whitens $\hat{\Sigma}$ rather than Σ_x, so this reading holds up to the scalar identified in Corollary 3.5 rather than as an identity.

E.5 Estimator and Preconditioner as One Object

AK-MOMENTUM is primarily a gradient estimator, and the preconditioning reading is what that estimator looks like when it is written in weight coordinates. Neither reading is only a statement

about the fixed point. What separates AK-MOMENTUM from EMA is the space in which the estimate is formed. A layer computes $y = Wx$, so a step $W \leftarrow W - \alpha M$ changes the output on input x by $-\alpha Mx$ while the loss asks for $-\alpha\delta$. The job of the buffer is therefore to estimate the map from input to desired output change, which is the regression of δ on $\hat{x}$. That is Definition 3.3, minimized by $\hat{G}\hat{\Sigma}^{-1}$, and (6) is online SGD on it. EMA estimates the raw weight-space gradient instead, which is Definition 3.2, minimized by $\hat{G}$. So $\hat{\Sigma}^{-1}$ is not an operator applied to a gradient after the fact. It is the normal equations of the regression that defines the estimate.

The preconditioning reading follows because weight space and function space are the same linear space under two inner products, $\langle A, B\rangle_F$ and $\mathbb{E}\langle A\hat{x}, B\hat{x}\rangle = \mathrm{tr}(A\hat{\Sigma}B^\top)$. The matrix $\hat{\Sigma}^{-1}$ converts between them, so writing the function-space estimate in weight coordinates produces the right-preconditioned form of Theorem 3.4. Substituting the buffer for EMA is appropriate because the two objectives are not in conflict. Both maximize the same linear functional $\mathbb{E}\langle\delta, M\hat{x}\rangle = \langle M, \hat{G}\rangle_F$, and they differ only in which norm is held fixed while doing so, $\|M\|_F$ for Definition 3.2 and the induced output change $\mathbb{E}\|M\hat{x}\|^2$ for Definition 3.3, with the Tikhonov term μ interpolating between them. The second constraint is the one the role of the buffer calls for, and for a linear layer the identification is exact. In expectation the substitution also cannot reverse a descent direction, since $((1-\beta)I + \eta\hat{\Sigma})^{-1} \succ 0$.

F Proofs for Linear Regression Dynamics

F.1 Per-Direction Iteration Matrices

Proof. The momentum update along u_i is, in expectation,

$$\text{EMA: } \mu_{t,i} = \beta\mu_{t-1,i} + (1-\beta)\lambda_i\, e_{t,i},$$
$$\text{Delta: } \mu_{t,i} = (\beta - \eta\lambda_i)\mu_{t-1,i} + \eta\lambda_i\, e_{t,i},$$

where Delta uses the conditional expectation $\mathbb{E}[M_{t-1}x_t x_t^\top \mid M_{t-1}] = M_{t-1}\Sigma_x$ projected onto u_i. The weight update is $e_{t+1,i} = e_{t,i} - \alpha\mu_{t,i}$. Substituting the momentum recurrence into the weight recurrence and arranging the state vector as $(e_{t,i}, \mu_{t-1,i})^\top$ gives (15) in the unnormalized reading.

For the deployed normalized-key algorithm the same derivation gives

$$\text{Delta: } \mu_{t,i} = (\beta - \eta\hat{\lambda}_i)\mu_{t-1,i} + \eta\kappa_i\, e_{t,i},$$

because the buffer is contracted by $\hat{\Sigma}$ while the injected value $\delta_t = E_t x_t$ still carries the raw input, so $\hat{G}u_i = \mathbb{E}[\delta\hat{x}^\top]u_i = -e_{t,i}\,\kappa_i$ with $\kappa_i = u_i^\top\mathbb{E}[\|x\|\,\hat{x}\hat{x}^\top]u_i$, using $x\hat{x}^\top = \|x\|\,\hat{x}\hat{x}^\top$. This is the form stated in (15), and it requires that $\hat{\Sigma}$ and $\mathbb{E}[\|x\|\,\hat{x}\hat{x}^\top]$ share eigenvectors. Only the trace moves. The determinant is $\tilde{\beta}_i$ either way, so Theorem 3.8 and Theorem F.2 are unaffected by the split. □

F.2 Per-direction Determinant Reduction

Proof. Direct computation. For EMA, $\det A_i^{\mathrm{EMA}} = \beta(1-\alpha(1-\beta)\kappa_i) - (-\alpha\beta)(1-\beta)\kappa_i = \beta - \alpha\beta(1-\beta)\kappa_i + \alpha\beta(1-\beta)\kappa_i = \beta$. For AK-MOMENTUM, $\det A_i^{\mathrm{Delta}} = \tilde{\beta}_i(1-\alpha\eta\kappa_i) - (-\alpha\tilde{\beta}_i)(\eta\kappa_i) = \tilde{\beta}_i - \alpha\eta\kappa_i\tilde{\beta}_i + \alpha\eta\kappa_i\tilde{\beta}_i = \tilde{\beta}_i$. The coupling κ_i cancels in both, which is why the determinant is set by the memory statistic alone. The inequality $\tilde{\beta}_i < \beta$ is immediate from $\eta\hat{\lambda}_i > 0$. The unnormalized reading is the same computation with κ_i replaced by λ_i and $\hat{\lambda}_i$ by λ_i. □

F.3 Convergence Rate Reduction in AK-MOMENTUM's Underdamped Regime

Lemma F.1 (Determinant lower bound on the spectral radius)**.** Let $A \in \mathbb{R}^{2\times 2}$ with $\det A > 0$. Then

$$\rho(A) \;\geq\; \sqrt{\det A}, \tag{22}$$

with equality if and only if the discriminant $\Delta(A) = \mathrm{tr}(A)^2 - 4\det A$ satisfies $\Delta(A) \leq 0$ (i.e., A has complex-conjugate eigenvalues or a repeated real eigenvalue).

Proof. Let z_1, z_2 be the eigenvalues, with $z_1 z_2 = \det A > 0$, so they are either both real with the same sign or a complex-conjugate pair. By the AM–GM inequality applied to $|z_1|, |z_2| > 0$,

$$\rho(A) = \max(|z_1|, |z_2|) \;\geq\; \tfrac{1}{2}(|z_1| + |z_2|) \;\geq\; \sqrt{|z_1||z_2|} = \sqrt{\det A}.$$

Equality in the second inequality holds iff $|z_1| = |z_2|$, which for a real matrix A holds iff either (a) $z_1 = z_2$ (repeated real eigenvalue, $\Delta = 0$), or (b) $z_1 = \bar{z}_2$ is a complex-conjugate pair ($\Delta < 0$). □

Theorem F.2 (Per-direction rate reduction in the underdamped regime)**.** *Assume the stability condition $\eta\hat{\lambda}_i < \beta$ (so $\tilde{\beta}_i = \beta - \eta\hat{\lambda}_i > 0$). Suppose that along the eigendirection $\hat{u}_i$ of $\hat{\Sigma}$, the normalized* AK-MOMENTUM *operates in the underdamped regime, i.e. $\Delta_i^{\mathrm{Delta}} < 0$. Then,* regardless of EMA's regime*,*

$$\rho_i^{\mathrm{Delta}} \;=\; \sqrt{\beta - \eta\hat{\lambda}_i} \;<\; \sqrt{\beta} \;\leq\; \rho_i^{\mathrm{EMA}}. \tag{23}$$

The reduction is anisotropic, since directions with larger directional density $\hat{\lambda}_i$ enjoy a strictly larger reduction.

Proof. Under stability, $\det A_i^{\mathrm{Delta}} = \tilde{\beta}_i > 0$ and $\det A_i^{\mathrm{EMA}} = \beta > 0$ (Theorem 3.8). Since $\Delta_i^{\mathrm{Delta}} < 0$, the eigenvalues of A_i^{Delta} form a complex-conjugate pair with squared modulus $\det A_i^{\mathrm{Delta}}$, hence $\rho_i^{\mathrm{Delta}} = \sqrt{\tilde{\beta}_i} = \sqrt{\beta - \eta\hat{\lambda}_i}$. By Lemma F.1 applied to A_i^{EMA}, $\rho_i^{\mathrm{EMA}} \geq \sqrt{\det A_i^{\mathrm{EMA}}} = \sqrt{\beta}$, with equality only if EMA is also underdamped or critically damped along $\hat{u}_i$. Since $\eta\hat{\lambda}_i > 0$, $\sqrt{\beta - \eta\hat{\lambda}_i} < \sqrt{\beta} \leq \rho_i^{\mathrm{EMA}}$. □

Remark F.3 (Explicit underdamped condition)**.** The discriminant of A_i^{Delta} is $\Delta_i^{\mathrm{Delta}} = (1 + \tilde{\beta}_i - \alpha\eta\kappa_i)^2 - 4\tilde{\beta}_i$, so the underdamped condition $\Delta_i^{\mathrm{Delta}} < 0$ is equivalent to

$$\alpha\eta\kappa_i \;\in\; \Big((1 - \sqrt{\tilde{\beta}_i})^2,\; (1 + \sqrt{\tilde{\beta}_i})^2\Big). \tag{24}$$

The window has width $4\sqrt{\tilde{\beta}_i}$, approaching 4 as $\tilde{\beta}_i \to 1$, so the band is wide whenever $\tilde{\beta}_i$ is not far from 1. The same calculation with $\tilde{\beta}_i \to \beta$ yields the EMA condition $\alpha(1-\beta)\kappa_i \in ((1-\sqrt{\beta})^2, (1+\sqrt{\beta})^2)$, and for matched (α, β) the two regimes share the same directions to leading order in $\eta\hat{\lambda}_i$, so Theorem F.2 applies on exactly the directions where EMA is also underdamped, which is the comparison of interest. For AK-AdamW the relevant α in (24) is the per-direction *effective* step size $\alpha/(\sqrt{v_i} + \varepsilon)$; under μP this is $\Theta(1)$ on hidden weights, comfortably inside the band along the directions on which loss-curve dynamics are non-trivial.

Regime of validity. Theorem F.2 restricts the comparison to the regime where AK-MOMENTUM is underdamped along $\hat{u}_i$, and EMA may be in any regime. Two remarks. *(i) Practical relevance.* High-density directions ($\hat{\lambda}_i$ near 1) typically operate in this regime under reasonable hyperparameters, and these directions dominate early- and mid-training loss-curve dynamics, making Theorem F.2 the operative regime in practice. *(ii) Honest scope.* When AK-MOMENTUM is overdamped along $\hat{u}_i$, the per-direction comparison depends jointly on trace and determinant, and a determinant decrease at fixed trace can in principle increase ρ.

G Proofs for Non-stationary Tracking Dynamics

G.1 Direction-selective Tracking under Distribution Shift

Proof. **EMA.** $\mathbb{E}[M_t \mid M_{t-1}] = \beta M_{t-1} + (1-\beta)\bar{G} = \bar{G} + \beta(M_{t-1} - \bar{G}) = M^* + \beta(M_{t-1} - M^*)$. Subtracting M^* and projecting onto u_i yields (16).

AK-MOMENTUM. From (7), $\mathbb{E}[M_t \mid M_{t-1}] = M_{t-1}(\beta I - \eta\Sigma_k) + \eta\bar{G}_k$. Using the fixed-point identity $\eta\bar{G}_k = M^*[(1-\beta)I + \eta\Sigma_k] = M^* - M^*(\beta I - \eta\Sigma_k)$:

$$\begin{aligned}\mathbb{E}[M_t - M^* \mid M_{t-1}] &= M_{t-1}(\beta I - \eta\Sigma_k) + \eta\bar{G}_k - M^* \\ &= M_{t-1}(\beta I - \eta\Sigma_k) - M^*(\beta I - \eta\Sigma_k) \\ &= (M_{t-1} - M^*)(\beta I - \eta\Sigma_k).\end{aligned}$$

Projecting onto u_i and using $\Sigma_k u_i = \lambda_i u_i$ yields $\mathbb{E}[T_{t,i}] = \tilde{\beta}_i T_{t-1,i}$. □

G.2 Uniform Tracking-rate Bounds (Normalized Variant)

For completeness we record the direction-uniform tracking bounds for the normalized variant of AK-MOMENTUM. They follow directly from Theorem 3.10 and Proposition C.1.

Corollary G.1 (Uniform tracking-rate bounds, normalized variant)**.** *For the normalized variant,* $\hat{\lambda}_i \in [0, 1]$ *implies*

$$\beta - \eta \;\le\; \tilde{\beta}_i \;\le\; \beta \quad \textit{for all } i, \tag{25}$$

so the fastest-tracking direction contracts at rate $\beta - \eta$*, and the slowest is bounded above by EMA's uniform rate* β *(a width- and layer-independent guarantee). Moreover, the directional-density-weighted mean contraction rate is*

$$\sum_i \hat{\lambda}_i \tilde{\beta}_i \;=\; \beta - \eta \,\|\hat{\Sigma}\|_F^2, \tag{26}$$

which by Cauchy–Schwarz satisfies $\sum_i \hat{\lambda}_i \tilde{\beta}_i \le \beta - \eta/n$*, with equality iff* $\hat{\Sigma}$ *is isotropic. Anisotropy of* $\hat{\Sigma}$ *strictly improves the density-weighted mean tracking rate beyond the isotropic baseline* $\beta - \eta/n$*.*

Proof. The bracket (25) is direct from $0 \le \hat{\lambda}_i \le 1$. For the density-weighted mean, $\sum_i \hat{\lambda}_i \tilde{\beta}_i = \beta \sum_i \hat{\lambda}_i - \eta \sum_i \hat{\lambda}_i^2 = \beta - \eta \,\|\hat{\Sigma}\|_F^2$, using $\mathrm{tr}(\hat{\Sigma}) = 1$. The Cauchy–Schwarz inequality $1 = (\sum_i \hat{\lambda}_i)^2 \le n \sum_i \hat{\lambda}_i^2$ gives $\|\hat{\Sigma}\|_F^2 \ge 1/n$, with equality iff all $\hat{\lambda}_i$ are equal. □

H Scope of the Theoretical Assumptions

The results of Section 3 carry different amounts of assumption. This appendix states which one describes a training run.

Lemma 3.7 needs only the key second moment and is an exact property of the deployed update, so it carries to any architecture, loss, and data. Theorem 3.10 lets both $\hat{G}$ and $\hat{\Sigma}$ move, imposes no regime restriction, and gives strictly faster expected tracking-error contraction along every direction with positive input density. The runs of Section 4 live there, so Theorem 3.10 and not Theorem 3.4 is what describes them.

Theorem 3.4 is the only result that needs quasi-staticity, and it needs half of it. The assumption covers two quantities, $\hat{G}$ and $\hat{\Sigma}$, and $\hat{\Sigma}$ alone sets the per-direction decay rates. Drift in $\hat{G}$ only makes the buffer lag a moving target, which is the tracking error Theorem 3.10 already bounds. The real condition is therefore that $\hat{\Sigma}$ moves slowly compared with the buffer memory window τ_i of (14), which is at most 100 steps at $\beta = 0.99$. The condition is local in time. It asks that $\hat{\Sigma}$ hold still over one window and reapplies as the window slides, so Theorem 3.4 describes the current phase of training rather than the whole run. This is the same locality that K-FAC and Shampoo rely on when they reuse an input-side factor for tens to hundreds of steps. It holds most comfortably after warmup and is weakest early in training and under abrupt input shifts, which are the cases Theorem 3.10 covers.

The linear-regression analysis of Section 3.3 is idealized by design. It exhibits a clean setting in which a strict per-direction improvement can be proved exactly rather than accounting for transformer training, and we know of no comparable result separating momentum schemes on non-convex losses. What carries to a transformer is the mechanism and not the closed form, and Lemma 3.9 and Proposition 3.11 are the two statements that carry it. Appendix I works out what they give beyond the squared loss, and Section 4.2 measures on the real 24-layer run the quantities that Lemma 3.7 and Theorem 3.10 govern.

I Guarantees Beyond Standard Linear Regression

Section 3.3 proves a strict per-direction improvement on standard linear regression. This appendix shows that the guarantee survives in two settings that the main text does not cover, high-dimensional regression with $p > n$ and canonical generalized linear models including logistic regression. Section I.4 then treats the non-convex losses deep networks produce, which are reached through the

tracking result of Section 3.4 rather than through the determinant. Throughout we work in the deployed normalized-key update based on Remark 3.1.

One ratio organizes all three. Along direction u_i the delta rule forgets at $(1-\beta)+\eta\hat{\lambda}_i$ per step against EMA's $(1-\beta)$, a ratio of

$$1 + r_i, \qquad r_i := \frac{\eta\hat{\lambda}_i}{1-\beta}, \tag{27}$$

and every gain below comes from that one factor. It shortens the memory window, it speeds relaxation toward a moving target, it shrinks the steady lag bound, and it scales direction i of the implicit preconditioner $(\mu I + \hat{\Sigma})^{-1}$ by $1/(1+r_i)$, which lowers the effective condition number on the data span.

I.1 A Loss-Free Determinant Lemma

The per-direction iteration of (15) was derived for a squared loss, but its determinant never uses the loss. Making that explicit is what lets the same comparison run in every setting below.

Lemma I.1 (Loss-free determinant, restating Lemma 3.9)**.** Along u_i, one step maps the pair (parameter error, buffer component) through

$$A = \begin{pmatrix} 1-\alpha c & -\alpha\tilde{\beta}_i \\ c & \tilde{\beta}_i \end{pmatrix}, \tag{28}$$

where α is the step size and c is the per-direction coupling from the parameter error into the buffer, equal to η times the local curvature along u_i. This is (15) with c left arbitrary, and $c = \eta\kappa_i$ recovers it. Then

$$\det A = \tilde{\beta}_i \quad \text{for AK-MOMENTUM}, \qquad \det A = \beta \quad \text{for EMA momentum}, \tag{29}$$

for any c and any α. The determinant depends only on the memory statistic, never on the loss that produced c. Consequently, by Lemma F.1,

$$\min_{\alpha} \rho(A) = \sqrt{\det A}, \tag{30}$$

so the best achievable per-direction rate falls from $\sqrt{\beta}$ to $\sqrt{\tilde{\beta}_i}$ on every direction with $c > 0$, whatever loss produced it.

Proof. Direct computation gives $\det A = \tilde{\beta}_i(1-\alpha c) + \alpha\tilde{\beta}_i c = \tilde{\beta}_i$, and the same computation with $\tilde{\beta}_i$ replaced by β gives $\det A = \beta$. Neither retains c. Lemma F.1 gives $\rho(A) \geq \sqrt{\det A}$ whenever $\det A > 0$, with equality exactly when the discriminant is non-positive, and Remark F.3 shows the discriminant is non-positive on a band of αc of width $4\sqrt{\tilde{\beta}_i}$, which is non-empty, so the bound is attained at the tuned step size. □

We state the comparison as a bound on the best achievable rate rather than as a claim at fixed α. At a step size held fixed across the two methods, a smaller determinant does not by itself force a smaller spectral radius, since an overdamped iteration can move the other way, which is the same scope Theorem F.2 states.

I.2 High-dimensional Linear Regression

In the regime $p > n$, where p is the input dimension and n the number of samples, the guarantee survives and sharpens.

Off the key span the rule is inert. If $\hat{x}^\top u = 0$ for every observed key, then $\hat{\Sigma}u = 0$ and $\hat{G}u = \mathbb{E}[\delta(\hat{x}^\top u)] = 0$, so both the correction term and the gradient term vanish along u. Neither the EMA buffer nor the AK-MOMENTUM buffer puts mass on a direction the data has not queried, and the difference between them is confined to the queried subspace.

The fixed point stays well posed. Corollary 3.5 gives $M^* = \hat{G}(\mu I + \hat{\Sigma})^{-1}$, which is defined for rank-deficient $\hat{\Sigma}$, exactly the regime in which the unregularized whitening $\hat{G}\hat{\Sigma}^{-1}$ is undefined. The rule therefore regularizes on its own, with the ridge $\mu = (1-\beta)/\eta$ supplied by the decay rather than chosen separately.

The gain grows with spread. Over the queried directions the improvement is the ratio $(\mu+\hat{\lambda}_{\max})/(\mu+\hat{\lambda}_{\min})$, so it is largest when the queried spectrum is spread out, which is the typical spiked scenario in high dimension. A ceiling is available for the normalized variant alone, since $\hat{\lambda}_i \in [0,1]$ gives

$$\operatorname{cond}(\mu I + \hat{\Sigma}) \;\le\; \frac{\mu+1}{\mu} \;=\; 1 + \frac{\eta}{1-\beta}, \tag{31}$$

a bound that is independent of width, of layer, and of the data.

I.3 Canonical GLMs

For a canonical generalized linear model with inverse link f, the per-sample gradient is $(f(w^\top x) - y)x^\top$, which is the same key-value structure the method is built on. Theorem 3.4, Lemma 3.7, and Theorem 3.10 therefore hold unchanged, since their proofs use only $\hat{G}$ and $\hat{\Sigma}$ and never a squared loss.

For the rate, linearize the joint dynamics of the parameter error and the buffer at the optimum $w_\star$. The scalar curvature c of Lemma I.1 becomes the matrix

$$K = \mathbb{E}\big[f'(w_\star^\top x)\, x\hat{x}^\top\big] = \mathbb{E}\big[f'(w_\star^\top x)\, \|x\|\, \hat{x}\hat{x}^\top\big]\,, \tag{32}$$

which is symmetric and positive semidefinite, using $x\hat{x}^\top = \|x\|\,\hat{x}\hat{x}^\top$ and $f' > 0$ for canonical links. If K and $\hat{\Sigma}$ share eigenvectors they diagonalize together, so the system splits into one block per direction, each a copy of (28) with the matching eigenvalue of K in place of c/η, and Lemma I.1 applies block by block. The fixed-point and tracking statements need no such condition.

I.4 Nonlinear Deep Neural Network Training

For non-convex deep losses, tracking is the right tool, because Theorem 3.10 constrains the recursion that produces the buffer and places no condition on the loss surface, so convexity never enters. We strengthen it with two results, stated against each buffer's own target so that scale differences between the two targets do not confound the comparison. We claim no global rate.

Proposition I.2 (Steady lag, restating Proposition 3.11)**.** Suppose the target of the buffer drifts by at most Δ_i per step along u_i. Then the expected tracking error satisfies

$$\limsup_{t\to\infty} \|\mathbb{E}[T_{t,i}]\| \;\le\; \frac{\tilde{\beta}_i \Delta_i}{1-\tilde{\beta}_i} \qquad \text{against EMA's} \qquad \frac{\beta\Delta_i}{1-\beta}. \tag{33}$$

Since $\tilde{\beta}_i < \beta$ on every direction with positive input density and $t \mapsto t/(1-t)$ is increasing on $[0,1)$, the bound is strictly smaller there, and the relaxation-time ratio is $1 + r_i$.

Proof. By Theorem 3.10, one step contracts the tracking error by $\tilde{\beta}_i$, and the drift adds at most Δ_i before the contraction, so $\|\mathbb{E}[T_{t,i}]\| \le \tilde{\beta}_i(\|\mathbb{E}[T_{t-1,i}]\| + \Delta_i)$. The fixed point of this recursion is $\tilde{\beta}_i\Delta_i/(1-\tilde{\beta}_i)$ and the recursion is a contraction, so the limit superior is bounded by it. The EMA statement is the same argument with $\tilde{\beta}_i$ replaced by β, which is (16). Monotonicity of $t/(1-t)$ and $\tilde{\beta}_i < \beta$ give the comparison. The relaxation time is $1/(1-\tilde{\beta}_i)$ against $1/(1-\beta)$, a ratio of $((1-\beta)+\eta\hat{\lambda}_i)/(1-\beta) = 1 + r_i$. □

Corollary I.3 (Uniform lag)**.** *If the drift follows directional density, $\Delta_i = c_0\hat{\lambda}_i$, then the* AK-MOMENTUM *lag is bounded by $\beta c_0/\eta$ uniformly over directions, while EMA's grows linearly in the density as $\beta c_0\hat{\lambda}_i/(1-\beta)$.*

Proof. Substituting into Proposition I.2, the lag is $\tilde{\beta}_i c_0\hat{\lambda}_i/((1-\beta)+\eta\hat{\lambda}_i)$. Bounding the numerator by $\beta c_0\hat{\lambda}_i$ and the denominator below by $\eta\hat{\lambda}_i$ gives $\beta c_0/\eta$, which does not involve i. The EMA bound is $\beta c_0\hat{\lambda}_i/(1-\beta)$, which is linear in $\hat{\lambda}_i$. □

The bridge back to the loss. Split the estimation error into two parts, $M - \hat{G} = (M - M^*) + (M^* - \hat{G})$. The first term is the lag, which is how far the buffer trails its own moving target. Proposition I.2 lowers its steady bound on every direction and Corollary I.3 caps it where EMA's grows with the density. The second term is the designed preconditioning bias of Theorem 3.4 rather than an error. So Proposition D.1 turns reduced lag on the high-density directions, which Figure 3c shows dominate the input variance, into reduced first-order shortfall in the realized loss decrease. Section 4.2 is the empirical form of that bridge, since it measures the gradient-estimator quality, the function-space prediction error, and the input-feature conditioning on the real 24-layer run.

J Mixed-Modality Inputs

A natural question is what happens when the input features are of mixed types, such as tabular data, text, and images together, which carry different natural metrics. The short answer is that nothing in Section 3 changes, because AK-MOMENTUM acts inside a layer on post-embedding activations and never sees raw input types.

The theory is untouched. Every result in Section 3 uses the input distribution only through $\hat{\Sigma}$ and $\hat{G}$. The key second moment of a mixture is the density-weighted combination of the second moments of its components, so heterogeneous input produces a valid $\hat{\Sigma} \succeq 0$ and every statement holds for any such $\hat{\Sigma}$. Mixing modalities changes the key spectrum, which is the very thing the mechanism adapts to.

There is one metric, not several. On the input side, after the embedding every modality lives in the same activation space under the same inner product. Per-sample ℓ_2 normalization also removes residual scale and unit differences before they reach the buffer while preserving directional density, which is scale free by Proposition C.1. On the output side the loss enters only through δ, so a different loss or metric per modality changes what is stored, not how it is stored, and no theorem in Section 3 uses a particular loss. An embedding is needed only in the sense that any network already has one, so no extra machinery and no new theory are required. Our experiments span two modalities trained separately, and an interleaved study is noted as future work in Section 5.

K Interaction with the Second Moment of AdamW

The delta correction and the second moment of AdamW act on different structure, so they compose rather than duplicate. This appendix gives the argument in full. We present it as a discussion rather than as a theoretical claim, since the central step is a heuristic factorization that we do not prove and that is exact only under an independence assumption a trained network does not satisfy.

The two act in different bases. The second moment v is diagonal in the coordinate basis and rescales entries of the update. The delta correction is diagonal in the eigenbasis of $\hat{\Sigma}$ and rescales input directions. Key normalization keeps the roles apart, since $\hat{\Sigma}$ has unit trace and therefore carries direction only, leaving overall scale to Adam.

Where the input side enters each. Heuristically, under $g = \delta x^\top$ with δ and x independent, the second moment factorizes as $v_{ij} \approx \mathbb{E}[\delta_i^2]\,\mathbb{E}[x_j^2]$, so the input-side factor that Adam sees is the diagonal of the input second moment, while the delta rule uses all of $\hat{\Sigma}$. The two therefore coincide only when $\hat{\Sigma}$ is near isotropic or coordinate aligned. Figure 3a rules that out in our models, where the per-layer input-feature condition numbers sit between 10^4 and 10^{10} throughout training. The independence assumption behind the factorization does not hold in a trained network, which is why we do not state this as a claim, but the conclusion it points to does not depend on the assumption being exact, only on $\hat{\Sigma}$ being far from isotropic.

What the delta rule adds on top of the second moment. Both arms of every comparison in Section 4 use the unchanged AdamW second moment, so whatever the delta rule contributes is measured on top of the scaling of Adam. The separations reported in Section 4.2.3 are measured on the input-feature covariance, which v registers only through its diagonal, so they are outside what v can produce on its own.

The one place they overlap. The two do overlap in the overall size of M relative to $\sqrt{v}$. Learning-rate tuning absorbs that overlap, which is the reason the tuned peak rate for AK-AdamW sits more than ten times below the AdamW value rather than near it (Appendix T). We read the offset as a scale correction and not as evidence that the two preconditioners are competing for the same structure.

L Deployed AK-MOMENTUM Algorithm

This appendix states the algorithm that produces every number reported in Section 4, so that the cost analysis of Appendix M and the empirical claims refer to the same object.

Per linear layer, with a batch of N tokens giving normalized keys $\hat{X} \in \mathbb{R}^{N\times n}$ and output-side errors $\Delta \in \mathbb{R}^{N\times m}$, write

$$G = \frac{\Delta^\top \hat{X}}{N} \in \mathbb{R}^{m\times n}, \qquad \hat{\Sigma} = \frac{\hat{X}^\top \hat{X}}{N} \in \mathbb{R}^{n\times n}, \tag{34}$$

and update the buffer by

$$\boxed{M \;\leftarrow\; \beta M + \eta\big(G - M\hat{\Sigma}\big).} \tag{35}$$

This is the batch form of (6) with the normalized key. AK-AdamW then applies the unchanged AdamW machinery to M, that is the second moment $v_t = \beta_2 v_{t-1} + (1-\beta_2) g_t^{\odot 2}$ taken on the ordinary weight gradient, bias correction, decoupled weight decay, and the preconditioned update $\widehat{M}_t \oslash (\sqrt{\hat{v}_t} + \varepsilon)$. AK-SGD applies $\theta \leftarrow \theta - \alpha M$ directly.

Two implementation points matter for the cost.

The gradient term is free. Forming G costs the same as the weight gradient it replaces, and the standard AdamW second moment consumes that weight gradient anyway, so the only optimizer-specific work is the correction $M\hat{\Sigma}$. Appendix M counts exactly that.

The contraction order is chosen per layer. The product $M\hat{\Sigma}$ can be formed either as $M(\hat{X}^\top \hat{X})$, which builds the Gram matrix once and reuses it across every layer reading the same input, or as $(M\hat{X}^\top)\hat{X}$, which never materializes an $n \times n$ matrix. The first is cheaper for square and tall layers and the second for wide ones, and the dispatch rule is given in Appendix M. The second moment $\hat{\Sigma}$ is taken on a tensor the step already forms and adds no GEMM of its own.

M FLOPs Count and Measurement Setup

M.1 Notation and FLOP Convention

For a single linear layer $y = Wx$ with weight $W \in \mathbb{R}^{m\times n}$ where $m = d_{\text{out}}$ and $n = d_{\text{in}}$, batched over $N = B \cdot L_{\text{seq}}$ tokens, with B the batch size in sequences and L_{seq} the sequence length:

Symbol	Meaning	Shape
X	Input activations	$N \times n$
∇Y	Output-side gradient	$N \times m$
W	Weight matrix	$m \times n$
M	Momentum buffer	$m \times n$
V	Second-moment buffer (AdamW)	$m \times n$
$\hat{X}$	Row-normalized inputs, $\hat{x}_i = x_i/\|x_i\|_2$	$N \times n$
d	Transformer hidden dimension	—
γ	Gated-MLP expansion ratio, $d_{\text{ffn}} = \gamma\, d$	—
L_{seq}	Sequence length, distinct from the layer count L	—

We adopt the standard convention that one fused multiply-add (FMA) counts as 2 FLOPs. Hence a matrix multiply of an $a \times b$ and $b \times c$ matrix is counted as $2abc$ FLOPs.

M.2 Standard Linear-Layer FLOPs

The baseline cost of a linear layer (forward + backward, excluding the optimizer step since it is comparatively negligible) is

$$\mathrm{FLOPs}^{\text{layer}}_{\text{baseline}} = \underbrace{2mnN}_{\text{forward } Y=XW^\top} + \underbrace{2mnN}_{\nabla X=\nabla Y\, W} + \underbrace{2mnN}_{\nabla W=\nabla Y^\top X} = 6mnN. \tag{36}$$

M.3 The Normalized-Key AK-MOMENTUM Update

Definition M.1 (Normalized-Key AK-MOMENTUM)**.** The normalized-key delta-rule update is

$$\boxed{M_{t+1} = \beta\, M_t + \frac{\eta}{N}\Big(\nabla Y^\top \hat{X} - M_t\, \hat{X}^\top \hat{X}\Big),} \tag{37}$$

or per-sample,

$$M_{t+1} = \beta M_t + \eta\big(v_t - M_t \hat{x}_t\big)\hat{x}_t^\top, \qquad v_t \coloneqq \delta_t, \tag{38}$$

where $G_t = \delta_t x_t^\top$ is the per-sample gradient and $\delta_t = \partial\mathcal{L}/\partial y_t$.

The factored implementation evaluates (37) as

$$\Delta M = \tfrac{1}{N}\big(\nabla Y^\top \hat{X} - M\hat{X}^\top \hat{X}\big) \equiv \tfrac{1}{N}\big(\nabla Y^\top - M\hat{X}^\top\big)\hat{X}. \tag{39}$$

M.4 Per-Layer Cost of the Correction

The deployed update is (35), and Appendix L explains why only the correction $M\hat{\Sigma}$ is optimizer-specific. This subsection counts that correction per layer, then Section M.5 aggregates it over a block.

M.4.1 Cost of Key Normalization

Lemma M.2 (Normalization FLOPs)**.** Computing $\hat{X}$ from X costs

$$\mathrm{FLOPs}_{\mathrm{norm}}(n, N) = 3nN + 2N \approx 3nN. \tag{40}$$

Proof. Per row i, computing $\|x_i\|_2^2 = \sum_j x_{ij}^2$ takes n multiplies plus $n-1$ adds, which is $2n-1 \approx 2n$ FLOPs, the square root takes 1, the reciprocal takes 1, and scaling all n entries takes n multiplies. Aggregating over N rows gives $N(3n+2) = 3nN + 2N$. □

This is sub-leading against a single GEMM at $2mnN$ by a factor of $3/(2m)$, which is about 0.15% at $m = 1024$. The normalization is computed once per distinct input and shared by every layer reading it.

M.4.2 Two Contraction Orders and the Dispatch Rule

The correction $M\hat{\Sigma}$ admits two evaluation orders with different costs.

Gram order. Form $\hat{G}_{\mathrm{gram}} = \hat{X}^\top \hat{X}$ at $2n^2N + n^2$, then $M\,\hat{G}_{\mathrm{gram}}$ at $2mn^2$, for a total of $2n^2N + 2mn^2$ up to lower-order terms. The Gram matrix is formed once per distinct input and reused by every layer that reads that input, so the $2n^2N$ term is shared while the $2mn^2$ term is per layer. Its spectrum lies in $[0, N]$ before the $1/N$ scaling, so the product is numerically stable.

Through-N order. Form $M\hat{X}^\top$ at $2mnN$, then multiply by $\hat{X}$ at $2mnN$, for a total of $4mnN$, never materializing an $n \times n$ matrix.

Comparing the two leading terms, $2n^2N$ against $4mnN$, the Gram order is cheaper exactly when $n < 2m$. This gives the dispatch rule used throughout.

$$M\hat{\Sigma} \;=\; \begin{cases} M\,(\hat{X}^\top \hat{X}) & \text{if } n < 2m \quad \text{(Gram order)}, \\ (M\hat{X}^\top)\,\hat{X} & \text{otherwise} \quad \text{(through-}N\text{ order)}. \end{cases} \tag{41}$$

M.5 Per-Block Count and the Overhead Band

M.5.1 Baseline Per-Block FLOPs

A standard transformer block with a gated MLP of expansion ratio γ holds four attention projections at $d \times d$, two gated-MLP matrices at $\gamma d \times d$, and one down projection at $d \times \gamma d$. Using (36) for each,

$$\mathrm{FLOPs}_{\text{block}}^{\text{baseline}}(\gamma) \;=\; \underbrace{(24 + 18\gamma)\, d^2 N}_{\text{linear (QKVO + gated MLP)}} \;+\; \underbrace{12\, d L_{\text{seq}} N}_{\text{attention scores/values}} \;. \tag{42}$$

For the Llama-2 ratio $\gamma = 8/3$ the linear term is $72\, d^2 N$.

M.5.2 Aggregating the Correction

Applying (41) layer by layer, and sharing each Gram matrix across the layers that read the same input, gives the following.

Group	Shape	Order	d^2N coeff.	d^3 coeff.
W_Q, W_K, W_V	$d \times d$	Gram, shared over one input	2	6
W_O	$d \times d$	Gram	2	2
$W_{\text{up}}, W_{\text{gate}}$	$\gamma d \times d$	Gram, shared over one input	2	4γ
W_{down}	$d \times \gamma d$	through-N	4γ	0
Total			$\mathbf{6 + 4\gamma}$	$\mathbf{8 + 4\gamma}$

The first three rows each contribute one shared $2d^2N$ term rather than one per layer, because W_Q, W_K, W_V read one and the same input and $W_{\text{up}}, W_{\text{gate}}$ read another. Sharing applies to the Gram matrix only. The multiplication by M that follows it is per layer at $2mn^2$, which carries no factor of N and is what the d^3 column collects. The down projection maps the expanded hidden state back to the model width, so $m = d$ and $n = \gamma d$ there. Every gated MLP in use has $\gamma \geq 2$, which makes $n \geq 2m$, so this layer takes the through-N order at $4mnN = 4\gamma d^2 N$. Key normalization costs $3nN$ per distinct input by Lemma M.2, which over the four inputs above, of dimensions d, d, d, and γd, gives $(9 + 3\gamma)dN$. The block count is therefore

$$\Delta\mathrm{FLOPs}_{\text{block}}(\gamma) = (6 + 4\gamma)\, d^2 N \;+\; (8 + 4\gamma)\, d^3 \;+\; (9 + 3\gamma)\, dN. \tag{43}$$

The two lower-order terms enter the ratio as $(8 + 4\gamma)d/N$ and $(9 + 3\gamma)/d$, which at $N = 524{,}288$ tokens per step and our widths of 384, 1024, and 1792 move it by about a tenth of a percentage point, so the leading term is the block-level number.

M.5.3 The Overhead Band

Theorem M.3 (Per-block overhead of the deployed rule)**.** *Under the dispatch rule* (41) *with normalized keys, the per-block cost of the correction relative to the linear forward and backward of* (42) *is*

$$\boxed{f(\gamma) \;=\; \frac{6 + 4\gamma}{24 + 18\gamma},} \tag{44}$$

which is strictly decreasing on $\gamma \geq 0$ and therefore satisfies

$$22.22\% \;=\; \tfrac{4}{18} \;<\; f(\gamma) \;\leq\; \tfrac{6}{24} \;=\; 25.0\%, \tag{45}$$

with $f(8/3) = 50/216 = 23.148\%$ at the Llama-2 ratio used in all our models.

Proof. The ratio follows from (43) and (42) by dropping the two lower-order terms. The endpoints are $f(0) = 6/24 = 25.0\%$ and $f(\gamma) \to 4/18 = 22.22\%$ as $\gamma \to \infty$. Endpoints alone do not give a band, so we add that $f'(\gamma) = -12/(24 + 18\gamma)^2 < 0$ for every $\gamma \geq 0$, which makes f strictly decreasing and puts every value between the two. The down projection is the only layer whose order depends on γ, so the count above holds for $\gamma \geq 2$ and the attainable values sit in the lower part of the range. □

The band is what makes the cost predictable across architectures. Any gated-MLP shape lands inside a range of under three percentage points, so the block-level number barely moves when the expansion ratio changes. Every gated MLP in use has $\gamma \geq 2$, so the attainable values sit in the narrower range from 22.22% to $f(2) = 23.33\%$, and the 25.0% endpoint is the limit at $\gamma = 0$ rather than a shape any such block takes.

M.6 Realized Per-Step Overhead and Measurement Setup

Theorem M.3 is a block-level statement about linear layers. Three effects at finite scale place the realized per-step overhead below it.

1. the attention $\mathcal{O}(dL_{\text{seq}}N)$ term of (42) inflates the baseline at $L_{\text{seq}} = 2048$.
2. the embeddings and the output projection contribute to the baseline but receive no correction, since those groups use standard AdamW under our μP scheme.
3. the sub-leading d^3 and dN terms of (43) remain visible at finite scale.

All three enlarge the denominator of the overhead ratio without enlarging the numerator, and all three shrink relative to the leading d^2N term as width grows, which is why the realized number rises with scale toward the band.

Measurement setup. We do not estimate the realized overhead from the closed form. Our training suite carries a FLOP counter that instruments every GEMM in the step, including the correction and the normalization, and we report what it counts over the actual runs. Both models use $L = 24$, $d_{\text{head}} = 64$, $V = 32{,}000$, untied input and output embeddings, and $\gamma = 8/3$, with $B = 256$ and $L_{\text{seq}} = 2048$, hence $N = 524{,}288$ tokens per step. Step time is measured end to end on a single H200, averaged over the training horizon after warmup, with the same data order and batch shape in both arms.

Results.

Scale	d	d_{ffn}	Realized per-step FLOP overhead	Measured step time
67M	384	1024	$\mathbf{11.2}\%$	$1.177\times$ AdamW
370M	1024	2752	$\mathbf{17.4}\%$	$1.153\times$ AdamW
1B	1792	4785	$\mathbf{20.3}\%$	$1.179\times$ AdamW

The counted overhead rises with width across all three scales, from 11.2% to 20.3%, approaching the band of Theorem M.3 from below as the three finite-scale effects above shrink relative to the leading d^2N term. Measured step time does not follow the count monotonically, and the reason is where the correction runs. At 67M the correction GEMMs are small enough that launch overhead dominates, so the measured cost sits above the count. At 370M the correction is one large GEMM per layer routed to tensor cores, so its FLOPs run at higher throughput than the average FLOP in the step and the measured cost falls below the count. At 1B the correction is still routed to tensor cores, but its share of the step has grown enough that the throughput advantage no longer covers it, so the measured cost tracks the count again. Reported wall-clock numbers use a research-quality, non-fused implementation of the correction, and we expect the gap to the counted overhead to narrow with a fused backward and optimizer kernel.

What this costs at matched loss. Table 3 reports the end-to-end consequence, measured over the full horizon with identical data order and initialization in both arms. Averaged over the matched validation-loss levels past the crossing point, AK-AdamW reaches the same loss with 25.9% fewer FLOPs and 21.6% less wall clock at 67M, and 4.5% fewer FLOPs and 6.2% less wall clock at 370M. Figure 4 shows the wall-clock curves. Because the correction is paid from the first step, the two arms cross once on each cost axis and AK-AdamW is ahead of AdamW everywhere after that point. The cost curves are single-seed, since the per-seed spread in Figure 1 is a property of the loss trajectory and not of the cost of a step.

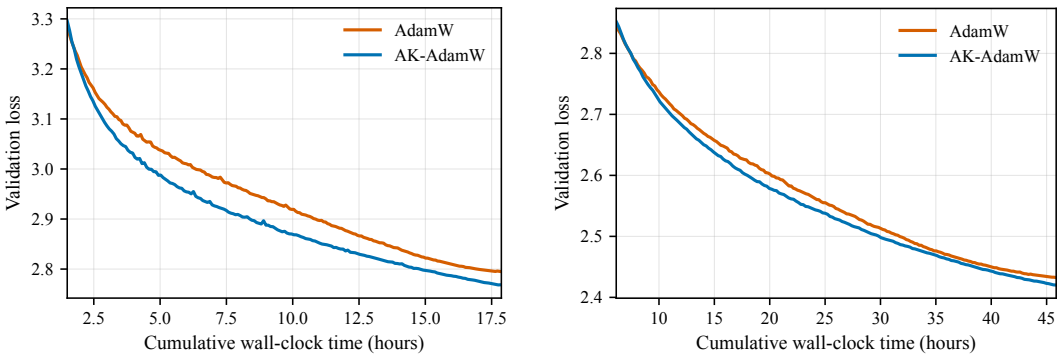

(a) 67M. (b) 370M.

Figure 4: Validation loss against cumulative wall clock on a single H200, single seed. AK-AdamW starts behind, because the correction is paid from the first step, crosses once, and is ahead for the rest of the run at both scales.

M.7 Peak-Memory Derivation

M.7.1 Persistent State

Optimizer	Buffers	Bytes/param (fp32)
SGD-momentum	M	4
AdamW	M, V	8
AK-SGD (norm-key)	M	**4**
AK-AdamW	M, V	**8**

Result M.4 (Persistent overhead = 0)**.** The persistent optimizer-state memory overhead of normalized-key AK-SGD against SGD-momentum, and of normalized-key AK-AdamW against AdamW, is exactly zero.

M.7.2 Saved Activations

The standard backward already saves X for ∇W. The factored delta also requires X (to build $\hat{X}$). Hence:

Result M.5 (Saved-activation overhead = 0)**.** No additional activation tensors must be saved between forward and backward.

M.7.3 Transient Memory During the Optimizer Step

Factored path.

Tensor	Shape	Bytes (fp32)
$\|x_i\|_2$	N	$4N$
$\hat{X}$	$N \times n$	$4Nn$
$T = M\hat{X}^\top$	$m \times N$	$4mN$
$R = \nabla Y^\top - T$	$m \times N$	in-place over T
U	$m \times n$	accumulates into M
Peak transient		$\mathbf{4Nn + 4mN + 4N}$

Gram path.

Tensor	Shape	Bytes (fp32)
$\|x_i\|_2$	N	$4N$
$\hat{X}$	$N \times n$	$4Nn$
$\hat{G}$	$n \times n$	$4n^2$
$C = M\hat{G}$	$m \times n$	accumulates
Peak transient		$\mathbf{4Nn + 4n^2 + 4N}$

For tall/square layers with $N \gg n^2/m$, the Gram path is strictly more memory-efficient. The cost from key normalization itself is the $4Nn$ term, but if we permit *in-place* replacement of X by $\hat{X}$ (the standard backward no longer needs X once $\hat{X}$ is formed and ∇W has been computed for Gram layers), this term is absorbed into the existing X allocation.

M.7.4 Per-Block Transient Peak Overhead

Under fused backward+optimizer execution (per-layer immediate update, no global ∇W retention across the network):

$$\boxed{\text{PeakMemOverhead}_{\text{block}}^{\text{norm-key}} \leq 4\,N \cdot n_{\max} \text{ bytes (fp32)}} \tag{46}$$

where $n_{\max} = \gamma d$ for the FFN-down input.

Result M.6 (Concrete peak overhead)**.** For $d = 1024$, $\gamma = 8/3$, fp16 storage, and a microbatch of $N = 8192$ tokens rather than the 524,288 tokens of a full optimizer step, since only one microbatch of $\hat{X}$ is live at a time, the largest normalized-key transient allocation is

$$2 \cdot 8192 \cdot (8/3) \cdot 1024 \approx 44.7 \text{ MB, per block.} \tag{47}$$

This is fully transient, since only one block's $\hat{X}$ is live at a time.

M.8 Theoretical Lower Bound

M.8.1 Sequential Read–Write Lower Bound

The delta rule's intrinsic operation per sample comprises:

1. *Read:* $\hat{v}_t = M_t \hat{x}_t$, costing $2mn$ FLOPs.
2. *Write:* $M \mathrel{+}= \eta(v_t - \hat{v}_t)\hat{x}_t^\top$, costing $2mn$ FLOPs.

Aggregating over N samples gives a lower bound of $4mnN$ for batched algorithms, or $2mnN$ for fully sequential ones, which is the through-N order of (41). The Gram order beats it whenever $n < 2m$ by moving the N contraction into a matrix that several layers share.

M.8.2 Tightness of the Asymptotic Result

The dispatch rule together with cross-layer Gram sharing yields (43), which is the theoretical minimum under three constraints, GPU-batched execution, a standard transformer architecture with no architectural relaxation, and independent block computation with no cross-block sharing. The leading coefficient $(6 + 4\gamma)$ saturates two structurally independent lower bounds at once, the per-layer read and write bound above and the Gram-shared bound from cross-layer input reuse. Further reduction would require relaxing one of the three, for example low-rank or sparse keys, a custom fused weight-gradient kernel, or cross-block input sharing, which the architecture does not allow.

N Experimental Setup

Architectures. Across all language modeling experiments we use a Llama-2-style [24] decoder-only transformer with SwiGLU FFNs (expansion ratio 2.67), rotary position embeddings (RoPE, base 10,000), pre-RMSNorm, no biases on linear layers, and untied input/output embeddings. Table 7 lists the three scales used in the main experiments. All three belong to the same width-only μP family: $d_{\text{head}} = 64$, $n_{\text{layers}} = 24$ and the SwiGLU expansion ratio are held fixed across scales so that scale enters only through d_{model}. The 67M model is the proxy at which all hyperparameters are tuned, and the 370M and 1B models are the μP transfer targets.

Table 7: Model architectures. All three belong to the same width-only μP family, with d_{head}, n_{layers}, and the SwiGLU expansion ratio fixed across scales, so scale enters only through d_{model}.

Scale	d_{model}	n_{layers}	n_{heads}	d_{head}	Vocab	Params
67M (proxy)	384	24	6	64	32,000	$\sim$67M
370M (target)	1024	24	16	64	32,000	$\sim$370M
1B (target)	1792	24	28	64	32,000	$\sim$1B

Data and training protocol. We pretrain on the 10BT subset of FINEWEB-EDU [17], tokenized with the Llama-2 SentencePiece tokenizer (vocabulary size 32,000). Sequence length is 2048 and the effective batch size is 256 sequences (524,288 tokens per optimizer step), giving 19,073 optimization steps for one full pass over the 10B-token budget. Training uses bfloat16 mixed precision, gradient norm clipping at 1.0, a cosine learning-rate schedule with linear warmup over the first 500 steps and decay to a floor of 10^{-2} of the peak rate, and no dropout. The validation set is a held-out 0.5% slice of FineWeb-Edu (not seen during training). The 1B run uses the 20BT budget, which is Chinchilla-optimal at that size, with the cosine cycle stretched to the longer horizon and the warmup held fixed at 500 steps, identically for both optimizers.

The matched-level measurement window. Every loss gap, step reduction, and cost saving we report is measured over matched validation-loss levels taken from step 2,000 onward, which is also the range the figures plot. The window drops the warmup and the transient right after it, where the two curves have not yet separated and a small difference in loss maps to a very large difference in steps, so a metric read there says more about the schedule than about the buffer. The window was fixed once, before any of the numbers below were computed, and the same window is applied at every scale, to every arm, and to both cost axes.

Baselines and AK-MOMENTUM instantiation. Our headline comparison is AK-AdamW against AdamW. AK-AdamW is obtained by replacing AdamW's first-moment EMA accumulator with the normalized-key AK-MOMENTUM update of Equation (37), and the second moment, bias correction, and decoupled weight decay are unchanged. The activations $\hat{x}_t$ and output-side error signals δ_t needed for the delta-rule innovation are captured per linear layer through forward and backward hooks, and the captured tensors are released immediately after the optimizer step (Appendix M). The pure delta limit ($\beta = 1$) is not used in our main runs, and we always operate with $\beta \in [0.9, 1)$ so that AK-MOMENTUM admits a uniform decay floor along every direction.

Hyperparameter selection via μP transfer. All hyperparameters are tuned on the 67M proxy and transferred to 370M and 1B via the μP scaling rules for hidden weights: $\text{lr}_{\text{eff}} = \text{lr}_{\text{proxy}} \cdot (d_{\text{base}}/d_{\text{model}})$ for both AdamW and AK-AdamW, while the delta coefficient η and the EMA coefficient β_1 transfer directly without rescaling. The η-invariance follows from the per-sample key normalization $\|\hat{x}_t\| = 1$ (Theorem Q.1 and Theorem C.2), and is verified empirically by a μP coordinate check at widths $\{128, 256, 512, 1024, 2048\}$ (Appendix S).

We use Optuna [1] with a TPE sampler and a SuccessiveHalvingPruner to search over learning rate, β_1, η (AK-AdamW only), and the auxiliary learning rate for the embedding and output-head group, with weight decay fixed at 10^{-1} and $\beta_2 = 0.99$. The auxiliary rate is tuned as its own axis for AK-AdamW and for Muon, because tying it to the main rate starves those parameters in both. AdamW uses one rate for all parameter groups, which is the standard configuration for it and the one its own μP rule expects, so it carries no separate auxiliary axis. Each trial trains the 67M proxy for 4,000 steps with the LR scheduler period set to the full 19,073-step horizon so that trial losses are comparable to early-training losses of the full run. Appendix T gives the final range of every axis, the pruner settings, the budget accounting, and the boundary audit. The configurations selected for the headline runs are listed in table 8.

Compute and seeds. All experiments are run on H200 GPUs (local cluster). A single 67M training run completes in roughly 36 GPU-hours on a single GPU, a 370M run completes in roughly 116 GPU-hours, and a 1B run completes in roughly 192 GPU-hours. These figures are the cost of running each configuration and not a throughput comparison across scales, because the microbatch size and the number of gradient accumulation steps differ by scale. The 370M runs leave GPU memory

Table 8: Optuna-selected hyperparameters at the 67M proxy and their μP-transferred values at the two targets. The η coefficient and β_1 do not rescale with width. "aux lr" is the auxiliary rate for the embedding and output-head group, tuned as its own axis.

optimizer	lr@67M	lr@370M	lr@1B	aux lr@67M	β_1	β_2	η	wd
AdamW	4.0×10^{-3}	1.5×10^{-3}	8.6×10^{-4}	—	0.95	0.99	—	0.1
AK-AdamW	3.0×10^{-4}	1.13×10^{-4}	6.4×10^{-5}	1.24×10^{-2}	0.99	0.99	0.37	0.1
Muon	8.0×10^{-3}	4.90×10^{-3}	—	1.28×10^{-2}	0.95	—	—	0.1

under-filled, since the next larger microbatch does not fit by a small margin, while the 1B runs fill memory more effectively at their own microbatch size, so cost per token does not fall out of model size the way a fixed microbatch would predict. The like-for-like timing comparison is the end-to-end step time of Section M.6, which is measured on a single H200 with the same batch shape in both arms. The 67M and 370M FineWeb-Edu comparisons are each repeated over 3 seeds (42, 777, 1234) for both AdamW and AK-AdamW, and we report per-seed bands at both scales. The Muon arm uses 3 seeds at each of 67M and 370M, with the same seed set (42, 777, 1234). The 1B comparison is single-seed because of compute, and we report it as a scale check rather than a significance claim. Reported wall-clock numbers use a research-quality, non-fused implementation of the delta-rule correction, and we expect the gap to the counted FLOP overhead (Section M.6) to narrow with a fused backward and optimizer kernel.

O Comparison with Structured Optimizers

This appendix reports the tuned Muon comparison in full and states why Shampoo and SOAP are absent. Section 4.1 summarizes the finding.

Table 9: AK-AdamW against a tuned Muon baseline on FineWeb-Edu, across matched validation-loss levels, in the same format as Table 2. Loss gap is in nats and step reduction is the fraction of Muon steps saved to reach the same loss, both reported as mean and maximum over the matched levels with the seed standard deviation. Matched levels are taken over the same step-2,000 window as Table 2.

Scale (seeds)	Mean loss gap	Max loss gap	Mean step red.	Max step red.
67M (3 seeds)	0.120 ± 0.008	0.140 ± 0.007	$49.4 \pm 2.4\%$	$55.8 \pm 1.9\%$
370M (3 seeds)	0.109 ± 0.003	0.132 ± 0.003	$41.6 \pm 0.8\%$	$48.1 \pm 0.7\%$

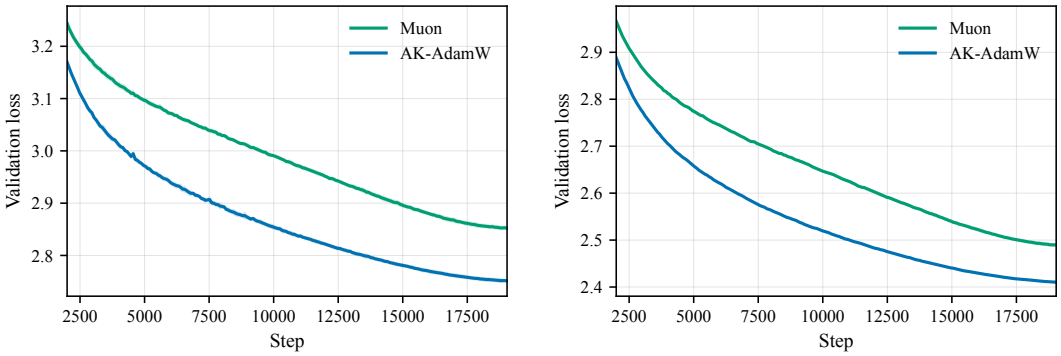

(a) 67M, 3 seeds.

(b) 370M, 3 seeds.

Figure 5: AK-AdamW against a tuned Muon baseline on FineWeb-Edu, validation loss against optimizer step, seed means with per-seed bands. The sign of the gap is consistent in every run, and the two curves do not cross at either scale.

Why AdamW is the isolating baseline. The empirical contribution of this paper is the delta-rule update applied to the first-moment buffer, and isolating it requires a baseline that differs from AK-AdamW only in that update. AdamW is the unique such baseline. A head-to-head against a structured

optimizer instead conflates the first-moment contribution with Newton–Schulz orthogonalization or with Kronecker-factored preconditioning, which act at a different level of the stack. That is why Section 4.1 leads with AdamW and treats Muon as a reference point rather than as the isolating comparison, and why the Muon numbers are reported here rather than beside the headline result.

Muon protocol. Muon was tuned under the same Optuna setup as the other two arms, with the same sampler, the same pruner, and the same trial horizon. Budgets were 33, 32, and 38 full-trial equivalents per tuned dimension for AdamW, AK-AdamW, and Muon, so Muon received the largest per-dimension budget of the three. Two further points make the tuning fair rather than merely equal in budget. Muon was tuned under its own μP rule, $\alpha = \Theta(n^{-1/2})$ with the $\sqrt{m/n}$ prefactor [19], rather than under an Adam-family rule [29], since transferring an Adam rule to a spectrally normalized update is not a like-for-like transfer. And the auxiliary AdamW learning rate for the embedding and output-head group was decoupled and tuned as its own axis for Muon exactly as for AK-AdamW. The 370M Muon run transfers the 67M champion with no re-tuning under that same rule, which is the protocol the other two optimizers also follow.

Scope of the Muon comparison. We make no general claim about Muon from Table 9. We report it as a baseline tuned inside our protocol rather than as a ceiling for the method.

Shampoo and SOAP. We did not run Shampoo or SOAP. Both keep a scalar-decay EMA first moment and add Kronecker-factored preconditioning on top of it, so the delta rule changes a different component of the stack and would slot into their buffers unchanged. The comparison that isolates our contribution is the EMA-against-delta swap at a fixed base optimizer, which is the argument of Appendix B, and we read Shampoo and SOAP as complementary rather than competing. The same holds for Muon, where the delta buffer would replace the EMA that feeds Newton–Schulz. AK-SHAMPOO, AK-SOAP, and AK-MUON are identified as future work in Section 5.

P Mechanistic Diagnostics of Momentum Dynamics

P.1 Explanation of Momentum–Gradient Cosine Similarity

The buffer–gradient cosine in stochastic optimization is *not* expected to approach $+1$, and is in general not even of definite sign. A Taylor expansion of $g_t = \nabla\mathcal{L}(\theta_t)$ around θ_{t-1} together with the update rule $\theta_t = \theta_{t-1} - \eta\, M_{t-1}/(\sqrt{V_{t-1}} + \varepsilon)$ yields

$$\langle M_{t-1}, g_t\rangle \;=\; \langle M_{t-1}, g_{t-1}\rangle \;-\; \alpha\,\frac{\langle M_{t-1}, H_{t-1}\, M_{t-1}\rangle}{\sqrt{V_{t-1}} + \varepsilon} \;+\; \langle M_{t-1}, \xi_t\rangle, \tag{48}$$

where $H_{t-1} \succeq 0$ is the local Hessian and ξ_t is stochastic gradient noise. The middle term is non-negative and biases $\cos(M_{t-1}, g_t)$ downward by an amount that depends on local curvature and step size, not on the buffer rule. This deterministic "stepping-rebound" effect applies symmetrically to EMA and AK-MOMENTUM, since it is a property of stochastic descent itself rather than of the optimizer. The diagnostic quantity is therefore the *gap between optimizers at matched training step*, and equivalently the prediction error e_t, which is monotone in $1 - \cos(M_t, g_t) \cdot \|M_t\|_F/\|g_t\|_F$.

Q Maximal-Update (μP) Scaling

We derive the width-scaling rule for the delta-rule coefficient η in the normalized variant under maximal update parameterization [29], showing that η is width-invariant and that the base optimizer's μP learning-rate rule is inherited unchanged. The analysis is presented for a single hidden linear layer, and the multi-layer extension follows by the same per-layer reasoning, since the delta-rule correction is layer-local.

Q.1 Setup and Per-Coordinate Scales

Consider a hidden linear layer $W \in \mathbb{R}^{m\times n}$ at width n with $m = \Theta(n)$. Under μP, the input $x \in \mathbb{R}^n$ has per-coordinate scale $\Theta(1)$, so $\|x\|^2 = \Theta(n)$ and the unit key satisfies $\|\hat{x}\|^2 = 1$ with per-coordinate scale $\Theta(n^{-1/2})$. The output-side error $\delta \in \mathbb{R}^m$ has per-coordinate scale $\Theta(1)$ for hidden

layers under μP. The gradient $g = \delta x^\top$ has per-coordinate scale $\Theta(1)$, and the EMA momentum buffer $M^{\mathrm{EMA}} = \mathbb{E}[g]$ has the same per-coordinate scale $\Theta(1)$.

Target scale for the AK-MOMENTUM buffer. The deployed algorithm uses the normalized key $\hat{x}$. The natural injection signal is $\eta\delta_t\hat{x}_t^\top$, which has per-coordinate scale $\Theta(\eta)\cdot\Theta(1)\cdot\Theta(n^{-1/2}) = \Theta(\eta/\sqrt{n})$. Setting $\eta = \Theta(1)$ gives a buffer with per-coordinate scale $\Theta(n^{-1/2})$. We show below that this is the consistent fixed-point scale under the recurrence (19) and that this scale matches the postprocessing requirements of each base optimizer, recovering the standard μP learning-rate rules.

Q.2 Width Invariance of η

Theorem Q.1 (μP width invariance of η)**.** *Under μP with input x of per-coordinate scale $\Theta(1)$ and output error δ of per-coordinate scale $\Theta(1)$, the normalized* AK-MOMENTUM *recurrence*

$$M_t = \beta M_{t-1} + \eta(\delta_t - M_{t-1}\hat{x}_t)\hat{x}_t^\top \tag{49}$$

admits a fixed-point per-coordinate scale of $\Theta(n^{-1/2})$ if and only if the delta-rule coefficient is width-invariant: $\eta = \Theta(1)$.

Proof. We track per-coordinate scales of M_t in steady state. Suppose M_{t-1} has per-coordinate scale s, i.e. $|M_{t-1,ij}| = \Theta(s)$. We compute the per-coordinate scale of each term in (49).

Decay term. βM_{t-1} has per-coordinate scale $\Theta(s)$.

Injection term. $\eta\,\delta_t\hat{x}_t^\top$ has per-coordinate scale $\Theta(\eta)\cdot\Theta(1)\cdot\Theta(n^{-1/2}) = \Theta(\eta/\sqrt{n})$.

Retrieval term. The vector $M_{t-1}\hat{x}_t \in \mathbb{R}^m$ has i-th coordinate $\sum_{j=1}^n M_{t-1,ij}\hat{x}_{t,j}$, a sum of n terms each of order $\Theta(s)\cdot\Theta(n^{-1/2}) = \Theta(s/\sqrt{n})$. Under random sign cancellation (the standard μP fluctuation argument applied to the inner product between a buffer row and the unit key), the magnitude of this sum is $\Theta(\sqrt{n}\cdot s/\sqrt{n}) = \Theta(s)$. Multiplying by $\eta\hat{x}_t^\top$ then gives per-coordinate scale $\Theta(\eta)\cdot\Theta(s)\cdot\Theta(n^{-1/2}) = \Theta(\eta s/\sqrt{n})$.

Fixed-point balance. At steady state $|M_t| = |M_{t-1}| = \Theta(s)$, so the largest term on the right-hand side of (49) must scale as $\Theta(s)$. Since the decay term is $\Theta(s)$ and the retrieval term is $\Theta(\eta s/\sqrt{n}) = o(s)$ for any $\eta = O(1)$, the binding constraint comes from the injection term: we need $\Theta(\eta/\sqrt{n}) = \Theta(s)$, giving $s = \Theta(\eta/\sqrt{n})$. For the resulting M_t to have a width-invariant per-coordinate *ratio* relative to its expectation, which is the standard μP feature-learning condition, we require $\eta = \Theta(1)$, hence $s = \Theta(n^{-1/2})$.

Conversely, if $\eta = \Theta(n^{-c})$ for any $c > 0$, the buffer scale becomes $\Theta(n^{-1/2-c})$, which violates feature learning. If $\eta = \omega(1)$, the retrieval term diverges relative to the decay term and stability fails. Hence $\eta = \Theta(1)$ is necessary and sufficient. □

Q.3 Inherited Base-optimizer Learning-Rate Rules

Corollary Q.2 (Inherited μP learning-rate rules)**.** *With $\eta = \Theta(1)$, the normalized* AK-MOMENTUM *buffer M_t has per-coordinate scale $\Theta(n^{-1/2})$, identical to the per-coordinate scale of the EMA momentum buffer (because EMA's buffer estimates the* population gradient *$\bar{G} = \mathbb{E}[\delta x^\top]$, whose per-coordinate expectation has scale $\Theta(n^{-1/2})$ under μP with random-sign cancellation, and the per-sample buffer scale is $\Theta(1)$ while its expectation exhibits the same $\Theta(n^{-1/2})$ shrinkage). Consequently, every postprocessing operation on M_t inherits the same scaling as it would under EMA, and the base-optimizer's standard μP learning-rate rule applies unchanged:*

- AK-SGD: *$\alpha = \Theta(1)$ for hidden layers, $\Theta(1/n)$ for output heads (matching SGD-with-momentum under μP).*
- AK-AdamW: *the preconditioned update $M_t/\sqrt{v_t + \varepsilon}$ has per-coordinate scale $\Theta(1)$ (because both M_t and $\sqrt{v_t}$ scale as $\Theta(n^{-1/2})$), so $\alpha = \Theta(1/n)$ for hidden layers, matching AdamW under μP.*

- AK-Muon: *the Newton–Schulz output* $\mathrm{NS}(M_t)$ *has unit singular values and per-entry scale* $\Theta(n^{-1/2})$ *for an* $m \times n$ *matrix with* $m = \Theta(n)$*, so* $\alpha = \Theta(n^{-1/2})$ *with the* $\sqrt{m/n}$ *prefactor of Muon, matching Muon under* μ*P.*

Proof. Per-coordinate scale of M_t is $\Theta(n^{-1/2})$ by Theorem Q.1. The Adam second moment v_t averages $g_t^{\odot 2}$, which has per-coordinate scale $\Theta(1)$ per sample but expectation scale $\Theta(n^{-1})$ under μP with random-sign cancellation, so $\sqrt{v_t} = \Theta(n^{-1/2})$ and $M_t/\sqrt{v_t} = \Theta(1)$. With this unit-scale preconditioned update, AdamW's standard μP learning-rate rule $\alpha = \Theta(1/n)$ for hidden weights gives $\alpha M_t/\sqrt{v_t} = \Theta(1/n)$ per coordinate, i.e. feature learning. Newton–Schulz produces an orthogonal-like matrix with unit singular values, and for an $m \times n$ matrix with $m, n = \Theta(n)$ this forces per-entry scale $\Theta(n^{-1/2})$, matching the standard Muon analysis. SGD without preconditioning uses $\alpha = \Theta(1)$ on the buffer of scale $\Theta(n^{-1/2})$, giving $\alpha M_t = \Theta(n^{-1/2})$ per coordinate, the standard μP feature-learning scale. □

Remark Q.3 (μTransfer)**.** Theorem Q.1 implies that η, once tuned at any width, transfers without rescaling to any other width. Combined with Corollary Q.2, this means the AK-MOMENTUM family is *μP-transparent*: it adds exactly one additional hyperparameter (η) over the base optimizer, and that hyperparameter requires no width-dependent scaling. We empirically verify width invariance of η via coordinate checks in Appendix S.

Remark Q.4 (Why normalization matters for μP)**.** The width-invariance of η rests on the unit norm $\|\hat{x}\| = 1$, which makes the spectral norm of the rank-one operator $\hat{x}_t \hat{x}_t^\top$ equal to 1 independently of n. For the unnormalized variant, $\|x\|^2 = \Theta(n)$, and the corresponding operator $x_t x_t^\top$ has spectral norm $\Theta(n)$, to maintain stability we would require $\eta = \Theta(1/n)$, which alters the steady-state scaling of M_t and the inherited base-optimizer learning-rate rule. The normalized variant avoids these complications entirely, and all μP scalings of the base optimizer carry over verbatim.

R Generality Across Optimizer Families and Architectures on CIFAR-10

This appendix complements Section 4.3 with full setup details and the corresponding test-accuracy comparison. We compare AK-SGD with momentum against vanilla SGD with momentum on a 3-hidden-layer MLP (4096, 4096, 2048 units per each layer, respectively, with ReLU activations) trained on CIFAR-10 [11] for 120 epochs at batch size 256. We manually sweep the learning rate independently for each optimizer over ($\alpha \in \{5 \times 10^{-2}, 1 \times 10^{-1}, 3 \times 10^{-1}\}$ for SGD and $\alpha \in \{0.9, 1.3, 1.7, 2.1\}$ for AK-SGD) and report the best configuration. The basin of α for SGD was found in $\alpha = 0.1$ as achieving the minimal loss, whereas for AK-SGD, $\alpha = 1.7$ was the identified learning rate achieving minimal loss, and the momentum coefficient β is swept within range $\{0.9, 0.95, 0.99\}$ for both optimizers, where $\beta = 0.9$ was preferable for SGD and $\beta = 0.99$ for AK-SGD. For AK-SGD we additionally search $\eta \in \{0.1, 0.5, 0.9, 0.99\}$ and find the optimal point in $\eta = 0.99$. Figure 6 shows the training and validation trajectories, and Table 10 reports final test accuracy.

Table 10: Final test accuracy on CIFAR-10 (3-hidden-layer MLP, 120 epochs). Best per-optimizer learning rate selected from an independent sweep.

Optimizer	Final test acc. (%)	Δ vs. SGD
SGD-momentum	61.51	—
AK-SGD	67.06	+5.55

The qualitative pattern matches the language-modeling result, since the gain appears early, is sustained throughout training, and translates into a positive final-metric difference. This experiment is a controlled test of whether the delta-rule mechanism transfers across optimizer families, run on a 3-layer MLP for that purpose, and the answer is positive.

R.1 Standard Vision Architectures

This subsection complements Section 4.3 and Table 4. We train ResNet-18 and ViT-Tiny on CIFAR-10 for 120 epochs, AK-AdamW against AdamW, with 3 seeds per optimizer and an identical log-scale

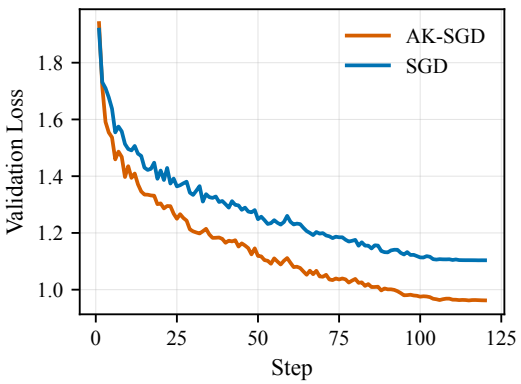

(a) Validation loss vs. epoch. The horizontal axis is the epoch index.

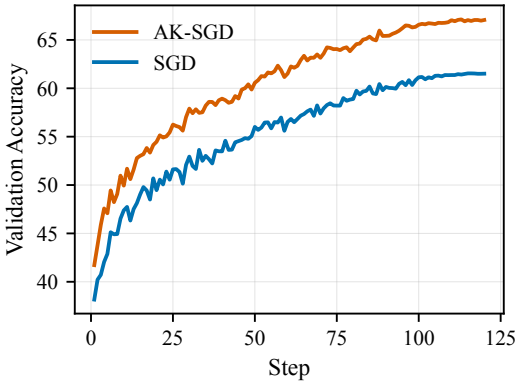

(b) Validation accuracy vs. epoch. The horizontal axis is the epoch index.

Figure 6: AK-SGD vs. SGD-momentum on CIFAR-10 with a 3-layer MLP. AK-SGD matches or exceeds SGD throughout training and achieves a higher final test accuracy, demonstrating that the delta-rule mechanism transfers beyond Adam's diagonal-preconditioner setting.

learning-rate sweep for each. All other settings are held at the values that the architecture's usual recipe prescribes and are the same across the two arms.

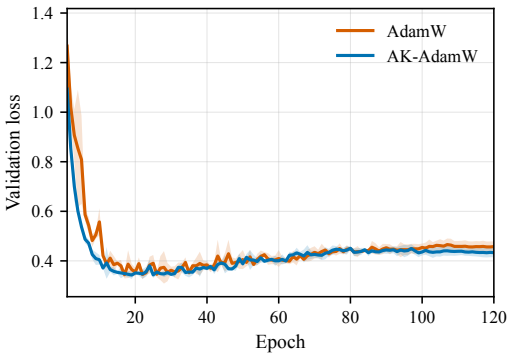

(a) ResNet-18, validation loss.

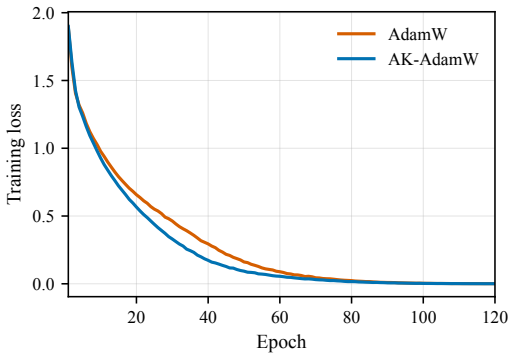

(b) ViT-Tiny, training loss.

Figure 7: AK-AdamW against AdamW on CIFAR-10 over 120 epochs, 3 seeds, seed means with per-seed bands. We read ResNet-18 on validation loss and ViT-Tiny on training loss, for the reason given below.

We read the two architectures on different curves, and the reason is what each curve can measure. ResNet-18 carries the locality and weight-sharing priors that CIFAR-10 rewards, so it generalizes well at this dataset size and its validation curve tracks optimization progress rather than a generalization gap. That makes validation loss both meaningful and the stricter of the two readings, so we use it. ViT-Tiny has no such inductive bias and is trained here from scratch without the large-scale pretraining or heavy augmentation that vision transformers normally rely on, so on a dataset of this size it fits the training set long before its validation loss reflects anything about the optimizer. Its validation curve is then dominated by the generalization gap of the architecture, which is a property of the model and not of the buffer rule, so we read ViT-Tiny on training loss, where the optimization question the paper asks is the one being measured. The complementary pair of curves is in Figure 8 and shows the same ordering in both cases.

We report the gap in training loss at matched epochs rather than a final metric, because both architectures saturate on CIFAR-10. Training accuracy reaches 99.99% and test accuracy sits near 84% for ViT-Tiny and 94% for ResNet-18 under either optimizer, so final performance cannot separate the two and convergence speed is the quantity that can be measured. We average over the phase in which the curves separate, which is roughly the first 60 epochs for ViT-Tiny and the first 20 for ResNet-18, and we report the gap both in nats and relative to the AdamW loss at the same

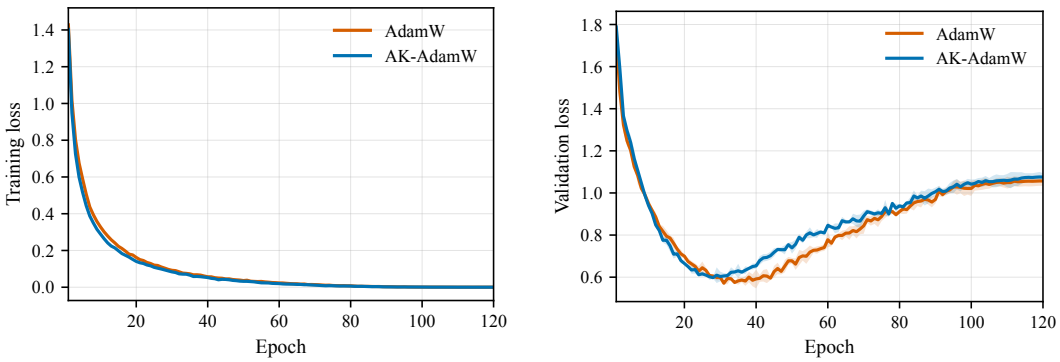

(a) ResNet-18, training loss.

(b) ViT-Tiny, validation loss.

Figure 8: The complementary pair to Figure 7, reported for completeness. The sign of the gap is the same here, and the ViT-Tiny validation curves show the generalization gap of the architecture on a dataset of this size rather than a difference between the optimizers.

epoch. The sign of the gap is the same in all runs, and validation loss shows the same ordering. This supports that the mechanism is not specific to language modeling, while language-model pretraining remains where the claims of this paper are made.

S μP Coordinate Check

Theorem Q.1 (Appendix Q) predicts that the delta-rule coefficient η is width-invariant under maximal-update parameterization. We verify this empirically with the standard μP coordinate-check protocol, training the same Llama-2-style architecture at five widths $d_{\text{model}} \in \{128, 256, 512, 1024, 2048\}$ for 20 optimization steps across five random seeds, holding all hyperparameters fixed except for the width-variant hyperparameters such as learning rate. In particular η and β_1 are transferred without rescaling, at $\eta = 0.5$ and $\beta_1 = 0.99$. The specific value of η is immaterial to this test, which asks only whether a single value transfers across widths, and it sits in the flat basin of Appendix U. We measured two per-coordinate scales whose width-invariance certifies μP-cleanness:

- **Activation RMS**: the root-mean-square per-coordinate magnitude of each layer's pre-activation, $\mathrm{RMS}(y_t) = (\frac{1}{m}\sum_i y_{t,i}^2)^{1/2}$, which should remain $\Theta(1)$ across widths.
- **Feature update RMS**: the per-coordinate magnitude of the change the realized weight update makes to the layer output, $\mathrm{RMS}(\Delta W x)$ with $\Delta W = W_{\text{after}} - W_{\text{before}}$, which should remain $\Theta(1)$ across widths under AK-AdamW's inherited μP learning-rate rule (Corollary Q.2).

Both quantities are measured in feature space, meaning projected onto the layer input, and that choice is deliberate. The parameter-space counterparts $\mathrm{RMS}(\Delta\theta)$ and $\mathrm{RMS}(\alpha\nabla W)$ are $\Theta(1/n)$ under correct μP and shrink with width, so a collapse test on them certifies nothing. The gradient is also the wrong proxy for the update here, since the second moment of Adam rescales it before it reaches the weights, so $\alpha\nabla W \neq \Delta W$ for the optimizers we compare. Taking the realized update and projecting it onto the input recovers the quantity the theory actually constrains. Under correct μP both scales are $\Theta(1)$ in width, so the curves for different widths should lie on one another, and a width-dependent trend in either one would open a spread that grows with n. We read the check by that collapse.

The collapse of the per-coordinate-scale curves across widths in Figure 9 confirms the theoretical prediction that a single η tuned at any width transfers without modification to any other width, with no degradation of feature-learning behavior. This is the practical content of Theorem Q.1.

T Hyperparameter Sweep

We use Optuna [1] with a TPE sampler and a SuccessiveHalvingPruner for hyperparameter selection on the 67M proxy. The search space, search budget, and selection criterion are summarized below.

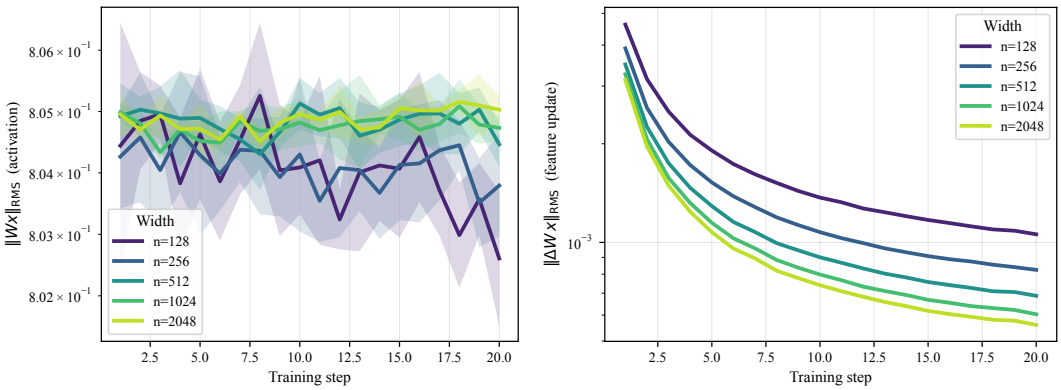

(a) Activation RMS vs. training step, by width.

(b) Feature update RMS vs. training step, by width.

Figure 9: μP coordinate check for AK-AdamW at widths $d_{\text{model}} \in \{128, 256, 512, 1024, 2048\}$ with η held fixed across widths. Both quantities collapse onto width-independent curves throughout the 20-step training horizon, empirically confirming that η requires no width-dependent rescaling and that the inherited μP scaling rule applies unchanged.

Search space. We run separate Optuna studies for AdamW, AK-AdamW, and Muon with single seed (42). We report the final range of each axis, which is the range the reported optimum was selected inside. Ranges were refit whenever an optimum approached a boundary, and each prior optimum was re-enqueued as an anchor trial before sampling resumed. For AdamW, $\alpha \in [2{\times}10^{-3},\ 8{\times}10^{-3}]$ on log scale and $\beta_1 \in \{0.9, 0.95\}$. For AK-AdamW, $\alpha \in [5{\times}10^{-5},\ 4.5{\times}10^{-4}]$ on log scale, $\beta_1 \in \{0.95, 0.99\}$, and η TPE-sampled from $[0.05,\ 1.0]$ on log scale. For Muon, $\alpha \in [3{\times}10^{-3},\ 3{\times}10^{-2}]$ on log scale and $\beta_1 \in \{0.9, 0.95\}$. For AK-AdamW and for Muon we additionally search the auxiliary AdamW learning rate for the embedding and output-head group as its own axis rather than tying it to the main rate, since tying it starves those parameters, over $[2{\times}10^{-3},\ 4{\times}10^{-2}]$ for AK-AdamW and $[2{\times}10^{-3},\ 5{\times}10^{-2}]$ for Muon. All studies hold $\beta_2 = 0.99$ and weight decay 10^{-1} fixed. Each trial trains the 67M proxy for up to 4,000 steps, evaluating every 80 steps, with the cosine LR scheduler period set to the full 19,073-step horizon so that trial losses are comparable to early-training losses of the headline run. The SuccessiveHalvingPruner uses `min_resource` $= 600$, `reduction_factor` $=$ 3, and `min_early_stopping_rate` $= 1$, which places exactly one rung inside the trial budget, realized at step $1{,}840$ of $4{,}000$. Champions are selected from full-budget completions only and never from rung values, because rung rank and final rank are close to uncorrelated among survivors in our studies.

Sweep budget. We count budget in full-trial equivalents, where one equivalent is one trial run to the full 4,000 steps, summing the steps every trial actually consumed. The AdamW studies ran 101 trials with 37 completions for 66.3 equivalents over 2 tuned dimensions, the AK-AdamW studies ran 207 trials with 72 completions for 129.2 equivalents over 4 dimensions, and the Muon studies ran 249 trials with 62 completions for 115.3 equivalents over 3 dimensions. Normalized by the number of tuned dimensions, the three arms received 33, 32, and 38 full-trial equivalents per dimension for AdamW, AK-AdamW, and Muon respectively. Muon therefore received the largest per-dimension budget of the three and our own method the smallest, which is the direction that matters for reading the comparison. Roughly 65 of the Muon trials are zero-cost prunes from a co-scheduling out-of-memory incident and consumed essentially no steps, leaving about 184 informative trials, and they are excluded from the equivalents above rather than counted as search effort. Most remaining trials are pruned, which is by design, since TPE concentrates samples near the basin and successive halving halts the rest at the rung. Total consumed compute is not equal across arms, since dimensionality and the number of refit rounds differ, so we claim identical protocol and per-dimension parity rather than equal GPU-hours. The Optuna SQLite study databases are released with the code.

Selection criterion. The objective is the validation loss at the end of each trial. The configuration with the lowest validation loss is selected for the headline run; no test-set information is used in selection.

Selected configurations. The selected hyperparameters at 67M and the corresponding μP-transferred values at the two targets are reported in Table 8. AdamW selects $\alpha = 4.0\times10^{-3}$ and $\beta_1 = 0.95$, and among the six completed AdamW trials all selected $\beta_1 = 0.95$. AK-AdamW selects $\alpha = 3.0\times10^{-4}$, $\beta_1 = 0.99$, and $\eta = 0.37$. Every completed AK-AdamW trial selected $\beta_1 = 0.99$, which is larger than AdamW prefers, and the recipe at the end of this appendix explains why the per-direction memory coefficient makes that the expected choice. The selected η sits inside the flat basin characterized in Appendix U, where the final loss moves by at most 0.015 nats across $\eta \in [0.10,\ 0.99]$, so neighbouring values in that basin do not change the headline configuration.

The AK-AdamW peak learning rate is more than ten times smaller than AdamW's, and this is consistent with the buffer scale. AK-MOMENTUM's per-coordinate buffer scale matches EMA's (Corollary Q.2), but the function-space objective induces a smaller effective gradient norm during the buffer-warmup phase, so the optimal α is correspondingly reduced.

Every reported optimum is interior to its final range, with completed trials on both sides of it, so no reported value rests on a boundary. Writing the position of each optimum as a fraction of its final range on the log axis, where 0 is the lower bound and 1 the upper, AdamW α sits at 0.51, AK-AdamW $(\alpha, \alpha_{\text{aux}}, \eta)$ at $(0.82, 0.61, 0.67)$, and Muon $(\alpha, \alpha_{\text{aux}})$ at $(0.43, 0.58)$. The horizontal bars in Figure 10 draw these ranges. Both categorical axes are resolved by completed evidence rather than by default, including a controlled probe at the adopted point on the other arm, and the β_1 selection is unanimous among the completed AK-AdamW trials.

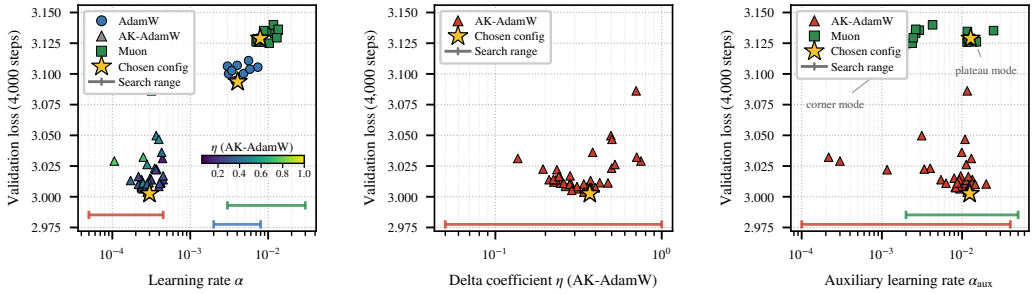

(a) Trial loss vs. main learning rate α. (b) Trial loss vs. delta coefficient η. (c) Trial loss vs. auxiliary rate α_{aux}.

Figure 10: Optuna trial losses on the 67M proxy, one point per completed trial, with the chosen configuration of each arm starred and the searched interval of each arm drawn as a horizontal bar. (a) The three arms occupy well-separated learning-rate basins, and each optimum is interior to its own final range with completed trials on both sides. (b) The η surface is flat over most of a decade, which is the trial-level counterpart of the sensitivity ablation in Appendix U. (c) The auxiliary rate for the embedding and output-head group separates into two modes. The corner mode collects trials that pin the auxiliary rate near the low end of the interval and starves those parameters, and the plateau mode collects the trials that do not, which is why we tune this rate as its own axis rather than tying it to the main rate.

Recommended tuning recipe. The marginal tuning cost over the EMA momentum is one coefficient. Based on the studies above, we recommend setting $\beta = 0.99$ and $\eta = 0.4$, keeping β_2 and weight decay at the AdamW settings, and setting the learning rate near one tenth of the tuned AdamW value and tuning only that. Three facts make this cost-efficient. First, $\beta = 0.99$ is larger than AdamW prefers, because the per-direction memory coefficient is $\tilde{\beta}_i$ rather than β, so every direction with positive input density forgets faster than nominal and a larger nominal β recovers the same effective horizon. Second, η is easy to select, since the final loss moves by at most 0.015 nats across $\eta \in [0.10, 0.99]$ (Appendix U) and η enters Theorem 3.4 only through the ridge μ, where the fixed point interpolates between the plain and the whitened gradient. Anything in $[0.3, 0.5]$ is a safe default. Normalized keys also remove any data-dependent constraint, since $\operatorname{tr}\hat{\Sigma} = 1$ places $\tilde{\beta}_i$ inside $[\beta - \eta, \beta]$ for any data, so $\eta \le \beta$ keeps every coefficient non-negative and stability needs only $\eta < 1 + \beta$. Third, the learning rate does not carry over from AdamW because the buffer is a Wiener predictor rather than an average of gradients. Both η and β are width-invariant under μP

(Theorem Q.1) and the learning rate is transferred by the standard μP rule, so the whole recipe is tuned once at the smallest proxy.

U η Sensitivity Ablation

Theorem 3.4 relates the regularization parameter $\mu = (1-\beta)/\eta$ to the fixed-point structure of the buffer, and this in turn predicts that final loss should depend smoothly on η, with $\eta \to \beta$ approaching the unregularized (pure delta-rule) Wiener fixed point. To verify this prediction and empirically characterize the role of η, we sweep η on the 67M proxy at the otherwise hyperparameters-fixed AK-AdamW configuration of Table 8. Each run uses batch size 256 and context length 2048 (524K tokens/step), trained for 5,440 steps ($\approx$ 2.85B tokens, $\approx 2.12\times$ Chinchilla optimal for this model size).

Table 11: Final validation loss on FineWeb-Edu (2.85BT, 67M proxy) as a function of the delta-rule coefficient η, with all other AK-AdamW hyperparameters fixed at the values in Table 8. The configuration selected by Optuna ($\eta = 0.37$) was chosen independently of this ablation and lies between the 0.30 and 0.50 grid points.

η	0.01	0.10	0.30	0.50	0.70	0.99
Final val. loss	3.063	3.029	3.034	3.035	3.035	3.020

The dependence on η is relatively flat for $\eta \geq 0.1$, with a wide basin that contains the selected value. The final loss varies by at most 0.015 nats across the wide interval $\eta \in [0.10, 0.99]$, and degrades smoothly at the limit ($\eta \approx 0$) while the pure-delta-rule limit ($\eta \to 1$) showed the best final validation loss by a small amount. Table 11 shows that $\eta = 0.99$ yields the lowest final loss in this $5{,}440$-step ablation, ahead of the 0.30 and 0.50 grid points that bracket the selected value by 0.014 and 0.015 nats and ahead of the next best point by 0.009 nats. Both margins are no larger than the 0.0150-nat seed standard deviation we measure on the 67M loss gap in Table 2, and this ablation is single-seed, so we do not interpret the $\eta = 0.99$ advantage as significant. This insensitivity is the practical correlate of the Tikhonov interpolation of Theorem 3.4, where a wide range of η produces buffers that interpolate between the EMA and Wiener targets without sharply changing the optimization behavior.

The ablation is run at the configuration of Table 8 with everything except η held fixed, so the sweep isolates η and any offset common to the row cancels in the spread. Its grid brackets the selected $\eta = 0.37$ between the 0.30 and 0.50 points, both of which sit in the flat basin. This is what makes the recipe of Appendix T safe to state as the interval $[0.3, 0.5]$ rather than as a point.

V Broader Impacts

AK-MOMENTUM is a general-purpose optimization method, not a deployed system. Its potential positive impact is improved training efficiency, which may reduce the compute cost of neural-network training and make experimentation more accessible. Its potential negative impact is indirect, since more efficient optimization could also lower the cost of training models for harmful or dual-use applications. The work does not release a high-risk model or dataset.